CHALMERS
UNIVERSITY OF TECHNOLOGY

Active Thermal Control of Power Semiconductor for High Power Electric Drive Applications

Master Thesis in Electrical Engineering

Master Thesis report in Sustainable Electric Power Engineering and Electromobility

AMARE YESGAT

DEPARTMENT OF ELECTRICAL ENGINEERING
CHALMERS UNIVERSITY OF TECHNOLOGY
Gothenburg, Sweden 2024
www.chalmers.se

Master's Thesis Report 2024

Active Thermal Control of Power Semiconductor for High Power Electric Drive Applications

AMARE YESGAT

Department of ELECTRICAL ENGINEERING
Chalmers University of Technology
Gothenburg, Sweden 2024

Active Thermal Control of Power Semiconductor for High Power Electric Drive Applications
AMARE YESGAT

© AMARE YESGAT, 2024.

Supervisor: Nimananda Sharma.,Chalmers, Department of Electrical Engineering
Examiner: Yujing Liu,Chalmers, Department of Electrical Engineering

Master Thesis 2024
Department of ELECTRICAL ENGINEERING
Chalmers University of Technology
SE-412 79 Gothenburg
Sweden
Telephone +46 76 4173128

Cover:

Gothenburg, Sweden 2024

Active Thermal Control of Power Semiconductor for High Power Electric Drive Applications
AMARE YESGAT
Department of Electrical Power Engineering
Chalmers University of Technology

Abstract

Electric vehicle applications, driven by the need for space and mass savings, increasingly demand high-power density inverters. However, this reduction in mass has led to a decrease in thermal capacity, badly exposing power semiconductors to larger temperature swings and thermal cyclic stress. The vulnerability of wire bonds and chip solder in the power semiconductor to failure due to thermal cycling necessitates a solution. This solution, actively controlling the junction temperature during operation, is the focus of this research and is referred to as active thermal control techniques (ATC).

Different active thermal control strategies are explored in the literature via manipulation of losses or heat dissipation and they are discussed in this work. Some of the methods require specific hardware, such as specialized gate drivers. The control of junction temperature without any extra hardware can be achieved by controlling the PWM frequency, load current, and modulation methods. However, controlling load current requires implementing an online current reference estimation. Additionally, changing the modulation method would increase control complexity. Therefore, this work investigates active junction temperature control by varying the PWM frequency.

The junction temperature is controlled using a hysteresis band-type controller with some modifications. The influence of the control band and average junction temperature calculation on the inverter's control effectiveness, prolonged lifetime, and improved efficiency is investigated. The inverter's losses are calculated analytically, and the inverter is implemented together with a heavy-duty truck and machine model in simulations. Drive cycle-based analysis is combined together with rain flow counting and a lifetime model to estimate the influence of the controller on the devices' lifetime. Simulation results show that the active control of the junction temperature can result in more than 246% increase in lifetime and simultaneously increase efficiency by 0.30%.

Keywords: lifetime, active thermal control (ATC), junction, junction temperature, thermal cycle, hysteresis controller.

Acknowledgements

Above all, I would like to thank the All-Powerful God, who has guided me throughout my life and provided me with the bravery and wisdom necessary to complete this thesis. I would like to express my deep gratitude to my adviser, Nimananda S., for his continuous support, encouragement, and priceless comments in thee whole period of this thesis work. I also would like to thanks to Yujing L., whose assistance as my examiner and attempts to resolve many issues were essential to the accomplishment of this job. I would also like to express my gratitude to my family and friends for their unwavering support and help during this path. Their support and encouragement have been invaluable in helping me to get through the difficulties.

Amare Yesgat
Gothenburg, October 2024

List of Abbreviation

PWM Pulse Width Modulation
ADC Analog-to-Digital Converter
AC Alternating Current
ATC Active Thermal Control
DC Direct Current
DCB Direct Copper Bonding
DPWM Digital Pulse Width Modulation
DSP7 Digital Signal Processor
EESM Electrically Excited Synchronous Motor
EV Electric Vehicle
FSW Switching Frequency
FT60 Flat Top 60 Degrees
GEVO Global EV Outlook
HHDDT Heavy Heavy-Duty Diesel Trucks
HTGB High-Temperature Gate Bias
HTRB High-Temperature Reverse Bias
IDSS Drain-Source Saturation Current
IEA International Energy Agency
IGBT Insulated Gate Bipolar Transistor
IGSS Gate-Source Leakage Current
MHD Magnetohydrodynamic
MOSFET Metal-Oxide-Semiconductor Field-Effect Transistor
NBTS Negative Bias Temperature Stress
PMSM Permanent Magnet Synchronous Motor
PI Proportional-Integral
PWM Pulse Width Modulation
Rds_on On-State Resistance
Si Silicon
SiC Silicon Carbide
SiO_2 Silicon Dioxide
T_J Junction Temperature
TDDB Time-Dependent Dielectric Breakdown
Vds_on Drain-Source On-State Voltage
V_th Threshold Voltage
VSI Voltage Source Inverter
ZCS Zero Current Switching
ZVS Zero Voltage Switching
1-D One Dimensional

Contents

List of Abbreviation **vi**

List of Figures **xiii**

List of Tables **xv**

1 Introduction **1**
1.1 Background 1
1.2 Aim 3
1.3 Scope 3
1.4 Limitations 3
1.5 Contribution 3
1.6 Research questions 4

2 Failure Types and Active Thermal Control Review **5**
2.1 Different Failures Type and Effects On MOSFET 5
2.1.1 Chip Level Failures Cause and Reference Parameters 6
2.1.2 Package Level Failures Cause and Reference Parameter 6
2.2 Active Thermal Control Strategies, ATC 8
2.2.1 Load and switching control 8
2.2.2 Active Cooling Mechanisms (fan and magnetohydrodynamic) . 19
2.2.3 Sensing and Feedback Control 19
2.2.4 Software Based ATC summery 19

3 System Modeling for ATC **25**
3.1 Analytical Power Loss Calculation 25
3.1.1 Switching loss 26
3.1.2 Conduction loss 27
3.2 Junction Temperature Estimation and RC Thermal Network 28
3.3 Rain Flow Counting 29
3.4 Life Time Modeling 30
3.5 Drive Cycle 35
3.6 Vehicle Model 37
3.7 Machine Model 37
3.8 PWM Frequancy Based Hystresis Controller 39

4 Analysis of ATC via PWM frequency **41**

4.1 Comparison With and Without Controller 41
4.2 Reference Temperature Band selection 44
4.3 Low Pass Filter Frequency selection 46
4.4 Sensitivity Analysis 49
4.4.1 Sensitivity to Different Lifetime Model 49
4.4.2 Sensitivity to Another Semiconductor Model 51
4.4.3 Sensitivity to Different Machine Model 54

5 Conclusion and Recommendation **57**
5.1 Conclusion 57
5.2 Recommendation 57

Bibliography **59**

A Appendix 1 **I**

List of Figures

1.1 Electric car sales per year[2] 2

2.1 Failures type of SiC MOSFET [11] 6
2.2 Solder layer and bond wires connection [11] 7
2.3 Failures type reviewed papers proportion[11] 8
2.4 Load current control for desired voltage reference [48] 11
2.5 Load current based frequency control [49] 11
2.6 Region definition for different temperature profile [53] 12
2.7 Sinusoidal PWM signal 13
2.8 Flat top 60 PWM signal 14
2.9 Hysteresis frequency controller [49] 14
2.10 Adaptive IGBT gate drivers [61] 16
2.11 Gate voltage control active control mechanism [60] 17
2.12 Turn-off trajectory adjustment circuit (TTAC) [64] 18
2.13 Schematic of half-bridge converter with split DC supply [65] 18

3.1 System model in block diagram 25
3.2 First-order (1-D) cauer type thermal network 28
3.3 Thermal network impedance [6] 29
3.4 Rain flow counting principle [82] 30
3.5 Histogram diagram with ten bins 31
3.6 Si and SiC,R. Bayerer et al. (CIPS 2008) model [7] 32
3.7 Si IGBT LESIT Project (1997) model [8] 33
3.8 Hybridpack SiC life time model [9] 34
3.9 Cruise and transient reference speed and acceleration 36
3.10 The d-q axis circuit representation of PMSM [83] 38
3.11 Hysteresis controller with analytic loss model integration 40

4.1 speed power, temperature and frequency 42
4.2 Transient mode only simulation result with controller 43
4.3 comparison of different temperature band 44
4.4 System result for 5 temperature band 46
4.5 power loss and junction temperature at different cutoff frequency . . . 47
4.6 System result at different controller frequency adjustment level . . . 48
4.7 Speed, total power loss, junction and average junction temperature . 50
4.8 Speed, total power loss, junction for six chip semiconductor Si lifetime model 53

4.9 Power loss, junction temperature and frequency comparison for EESM and PMSM machine 55

List of Tables

2.1 Failure and Characteristics summery in Power Electronic Devices [11] 9
2.2 Classification of ATC [10] 10
2.3 Classification of Hhardware ATC [10] 15
2.4 PWM frequency based Software ATC strategies 20
2.5 Load current based Software ATC strategies 21
2.6 DPWM frequency based Software ATC strategies 23

4.1 Comparison of Lifetime and Efficiency With and Without Controller Si IGBT, R. Bayerer et al. (CIPS 2008) model 41
4.2 Comparison of Lifetime and Efficiency With and Without Controller for transient model only 45
4.3 Simulation Results for Different Temperature Bands 45
4.4 Simulation Result for different cutoff frequencies 48
4.5 Simulation Results for different frequency increment 49
4.6 Comparison of Lifetime and Efficiency With and Without Controller SiC IGBT, R. Bayerer et al. (CIPS 2008) model 51
4.7 Efficiency and lifetime comparison of IGBT with and without for Si bond wire failures Lesit Project (1997) model 51
4.8 Efficiency and lifetime comparison of IGBT with and without for Si solde layer fatigue LESIT Project (1997) model 51
4.9 Efficiency and lifetime comparison of IGBT with and without controller for SiC hybridpack solder layer fatigue model 52
4.10 Efficiency and lifetime comparison of with and without controller for SiC hybridpack bond wire failure lifetime model 52
4.11 Six chip semiconductor With and Without Controller Si IGBT, R. Bayerer et al. (CIPS 2008) model 52
4.12 Six chip semiconductor With and Without Controller SiC IGBT, R. Bayerer et al. (CIPS 2008)lifetime model 52
4.13 The two chips comparison using Si IGBT, R. Bayerer et al. (CIPS 2008) lifetime model 54
4.14 The two chips comparison using SiC IGBT, R. Bayerer et al. (CIPS 2008) lifetime model 54
4.15 EESM With and Without Controller Si IGBT, R. Bayerer et al. (CIPS 2008)lifetime model 55
4.16 EESM With and Without Controller SiC IGBT, R. Bayerer et al. (CIPS 2008)lifetime model 56

4.17 EESM and PMSM comparison using Si IGBT, R. Bayerer et al. (CIPS 2008)lifetime model 56
4.18 EESM and PMSM comparison using SiC IGBT, R. Bayerer et al. (CIPS 2008)lifetime model 56

1
Introduction

1.1 Background

A lot of research has been carried out for a certain time in automotive industries, specifically electric cars. The first exhibition of discovers of electric vehicles was created in the 19th century by Thomas Davenport and Robert Anderson between 1820 and 1830. It has become popular over worldwide, even after a century. The sales of electric cars are growing very quickly year over year, according to the International Energy Agency(IEA) as shown from the figure blow [1].

Approximately one in five sales cars in 2023 were electric. Nearly 14 million electric automobiles were sold in 2023 .With the bulk of those sales taking place in China, Europe, and the US. About 14 million brand-new electric cars were registered worldwide in 2023. This is increasing the total number of automobiles on the road to 40 million. This amount largely corresponded with the Global EV Outlook 2023 (GEVO-2023) sales estimate. In 2023, 3.5 million more electric vehicles were sold than in 2022 which is a 35% annual increase. This is more than six times it was in 2018 which was only five years ago. There are more car registrations every week in 2023 than there were in 2013 whole year. The car sold in one weekly during 2023 is higher than the 2013 whole annual year total sold cars. In 2023 electric cars accounted for almost 18% of all sold vehicles which is up 2% from 2022 [2].Figure 1.1 shows that how the sale of electric car grow faster in a few consecutive years.

Based on to European forecast research, by the next decade, the growth rate will be more than a double or triple that of the present day. So, the study shows that by 2040, with the growth of electric vehicle sales. According to the research European countries will become the leaders of the production and sales market by producing sixteen million electric vehicles which followed by China and America, fabricating fourteen million electric cars each. This research implies that only the sales by China or America will be higher than electric car sales all over the world by 2023 and this shows that electric vehicles will take over fully any other non-electric vehicle and push out from the road by the near time [3].This rapid growth leads me to work on the electric vehicle area, especially on the inverter design and analysis, since the advancement in charging speed, decrease in the power loss of the electronic modules (MOSFET), and its lifetime extension can accelerate its rapid growth rate.

Most electric vehicle manufacturer uses high voltage rating batteries and well-

developed inverters (MOSFET) to handle and accomplish some advantages.Those advantages are reduction of charging cable size and reduced complexity, high power density, switching loss reduction and short charging time, lighter wires, and more efficient motors, However, this high-voltage battery creates stress on power semiconductors, and therefore, the reliability, lifetime, and proper functionality of the power semiconductors becomes questionable.Increasing energy density is also in demand in electric vehicle.this reduce the thermal capability and increase junction temperature.

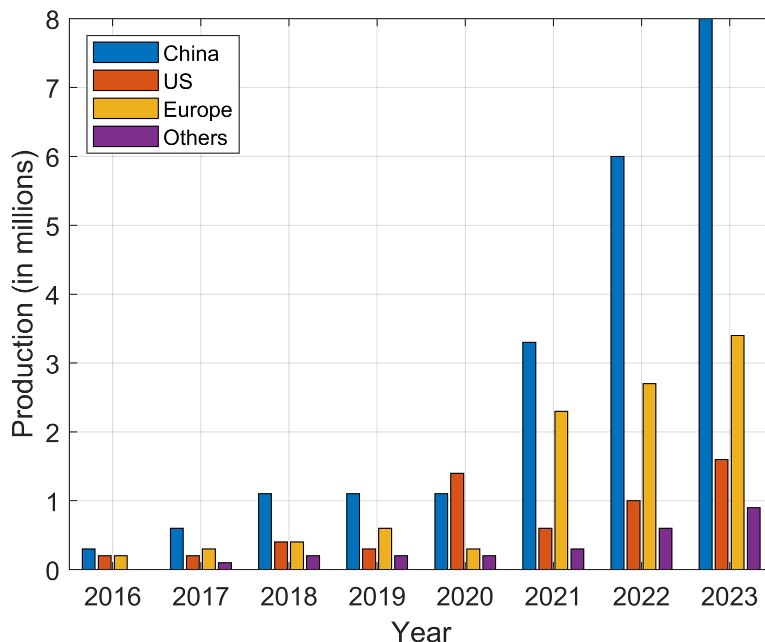

Figure 1.1: Electric car sales per year[2]

Despite the rapid increases in electric vehicle use, those thermo-mechanical stresses on power semiconductors hinder rapid growth.The stress is due to the power loss fluctuation. This causes increases in the junction temperature, especially at the bond wire and solder layer of the power semiconductor, finally affecting its reliability and lifetime. Therefore, using the analytic model of the power loss and junction temperature model of the power semiconductor, it is necessary to handle the junction temperature swing by monitoring different parameters such as load current, switching frequency, duty cycle, and power factor [4].This thesis develops the analytic model of the power semiconductor by considering the switching and conduction loss and 1-D thermal network to determine the junction temperature of the Hybrid PACK™ Drive G2 module of SiC MOSFET [6, 11].By controlling the switching frequency, the effect of junction temperature on the reliability and lifetime of the power semiconductors are analyzed based on different lifetime models such as the LESIT project1997 model, R. Bayerer et al. CIPS 2008 model and another solder layer and bond wire-based lifetime models of Hybrid PACK™ Drive G2 module [7–9].

In order to maintain the switching and conduction loss at a regulated constant value,

active thermal control (ATC) strategies are required, which control different parameters of both types of losses in order to extend the lifetime and ensure reliability. There are various types of ATC mechanism, such as increasing overload capability, thermal cycle reduction, balancing the thermal stress of the power devices, and controlling the thermal stress of the devices in different building blocks. This thesis uses a thermal cycle reduction mechanism using a PWM switching frequency-based hysteresis controller by manipulating switching loss and conduction loss [10].

1.2 Aim

This project aims to analyze the effect of junction temperature variation on the reliability and lifetime of power semiconductors using the conduction and switching loss model. The design uses and considers the HybridPACK Drive G2 module with SiC and MOSFET module parameters, which is now highly used for high-voltage and high-power traction drive applications. Also, the junction temperature analysis is extended with the help of the different chip levels of power semiconductors, lifetime models, machines, and vehicle types.

1.3 Scope

The scope of this project is investigating the different methods of active thermal control, especially exploring software-based and MATLAB/SIMULINK simulations of analytic model with PWM frequency controller of power semiconductor devices used for drive applications. The simulation is subdivided into analytic models, junction temperatures, lifetime models, and drive cycle models.

1.4 Limitations

As stated in the scope this project works until the simulation and have not done experimental verification even though I use the some experimental results conducted by another related project and industrial data sheet parameter values like the HybridPACK Drive G2 Infineon module of MOSFET for comparison with the simulation.

1.5 Contribution

This project's findings and simulation results help as input and foundations for future studies on improving the reliability and lifetime of power semiconductors, especially bond wire failures and solder layer fatigue, and can be extended to experimental verification.

1.6 Research questions

Thesis research questions. How essential are active thermal control methods to handle the fluctuation of junction temperature and increase the lifetime of power semiconductors is the general research queastion. The first one is how much the junction temperature fluctuation affects the lifetime of power semiconductors. This research question is answered by analyzing the junction temperature variation through different lifetime models. Is the same temprature load profile have the same effect on different chip level of power semiconductor and different vehicle type is the second research question.

2

Failure Types and Active Thermal Control Review

This chapter has two main sections. The first one discusses the type, cause, result, and mechanisms of power semiconductor failures. After describing the failures, it is required to address the handling mechanism, so-called active thermal control, ATC. Therefore, the second subsection explores different types of ATC strategies by dividing them into three main categories. Finally, it summarizes the software-type ATC strategies.

2.1 Different Failures Type and Effects On MOSFET

Most the failure of MOSFET comes from thermal and mechanical stress. All those factors lead to two different broad types of MOSFET failures: chip level failures, which occur on the chip components of MOSFET, and package level failures, which occur mainly in the joining or connecting layers of the MOSFET [11]. Gate oxide and body diode are the most frequently occurring chip level failures. Bond wire and solder layer are from package level failures. SiC MOSFET can have the capability of high voltage withstand, higher operating temperature, very fast switching frequency and reduced on-state resistance. But the chip level failures of SiC MOSFET are much more vulnerable than Si MOSFET due to the high requirement of electric field, temperature operation and a more minor conduction band cancellation between Silicon carbide and silicon dioxide [12–15] and, less flexibility and frequently affected by thermomechanical degradation due to coefficient of thermal expansion mismatch [16, 17].

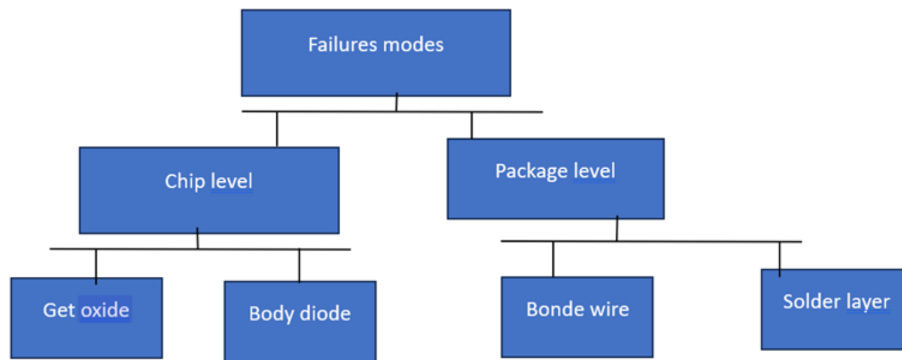

Figure 2.1: Failures type of SiC MOSFET [11]

2.1.1 Chip Level Failures Cause and Reference Parameters

A.Gate oxide failure: Driving current into the gate oxide layer in a small path is primarily responsible for gate oxide deterioration failure [18]. The deterioration of gate oxides is also caused by high electric field stress and high-temperature stress. Consequently time-dependent dielectric breakdown (TDDB) is increased and the high electric field also causes avalanche breakdown. In SiC MOSFETs the more likely deteriorated gate oxide will finally creates short circuits [19]. Some reference parameters show the deterioration of the gate oxide are miller plateau voltage amplitude, miller plateau time duration, drain leakage current and threshold voltage, gate leakage current, and on-state resistance [19]. The time duration of the gate-source voltage of the miller plateau also shows a clear time duration shift under high electric field stress [20, 21]. Under the high-temperature gradient bias (HTGB) test, both the threshold voltage Vth and the drain leakage current Idss tend to rise with stress time [22–24]. The high-temperature reverse bias (HTRB) test also shows that gate leakage current Igss rises with the high reverse bias temperature stress time [23]. Finally, Rdson is also the indicator of gate oxide deterioration under a high electric field by boosting its value since the electric field increases the oxide density [21, 24–27].

B.Body diode failure: The big factor contributing to body diode degradation is the high forward voltage bias stress. This stress causes the combination of stacking fault mechanisms. That results in high energy accumulation for hole and electron recombines and finally causes accumulation stack [28]. Which leads to body diode failure due to continuous current flow. The most common reference parameters for body diode degradation are on-state resistance [29], forward voltage [30], and drain leakage current [31].

2.1.2 Package Level Failures Cause and Reference Parameter

Bond wires connect the direct copper bonding (DCB) and silicon carbide die. The solder layer is typically used to connect the chip die and direct copper bonding and

also the base plate and direct copper bonding.

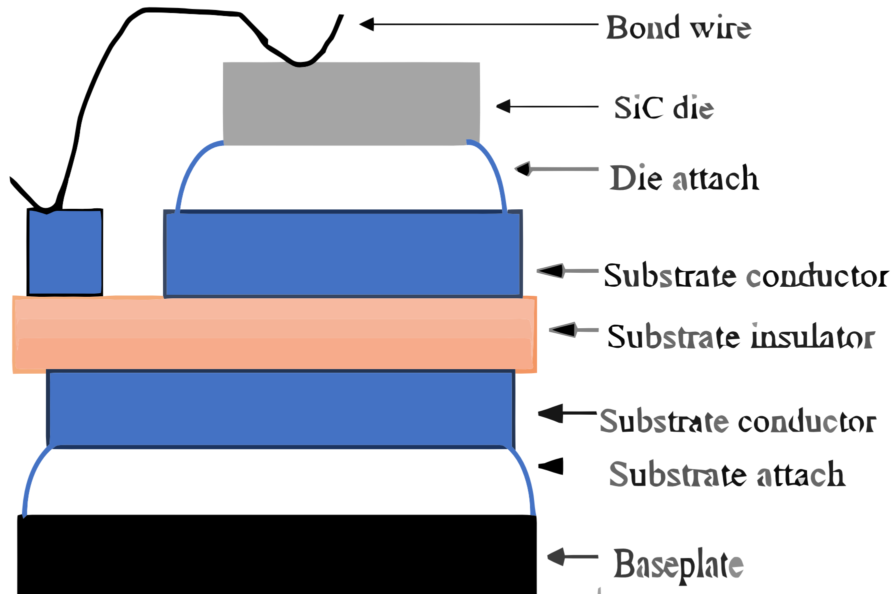

Figure 2.2: Solder layer and bond wires connection [11]

The package level failures occur most at the solder layer and at the bond wire area, which is mainly caused by the coefficient of thermal expansion mismatch among the different inter-connected components and finally come with an effect of solder fatigue, crack growth, and bond wire failure [32–34]. Humidity stress is another cause of package level failure, which accelerates the crack growth [35]. The small size of the SiC die is also highly affected to high current density stress, and this increases the (movement of atoms) electro-migration rate [35, 36]. Basically, there are two types of bond wire failure methods, which are bond wire fractures at the connecting point between the bond wire and DCB and the other is bond wire lift-off at the connecting point between bond wires and SiC die [37,38].The continuous time shifting between cooling and heating causes wire fractures .Whereas lift-off is caused by the temperature difference between bond wire copper and SiC die [36].

The lift-off type is the most frequently occurring bond wire failure [39] . Increasing of On state voltage [40, 41] and on state resistance [42] increases the bond wire resistance [36] and eddy current [43]. In the solder layer failure type, the coefficient of thermal expansion difference causes empty space and cracks after a long time. As a result, thermal resistance increases, and temperature rises.The junction to case thermal resistance [44] and solder layer resistance [45] are the reference parameter for the solder layer failures. The table 2.1 below shows the failures type with their reference parameter and failure place.

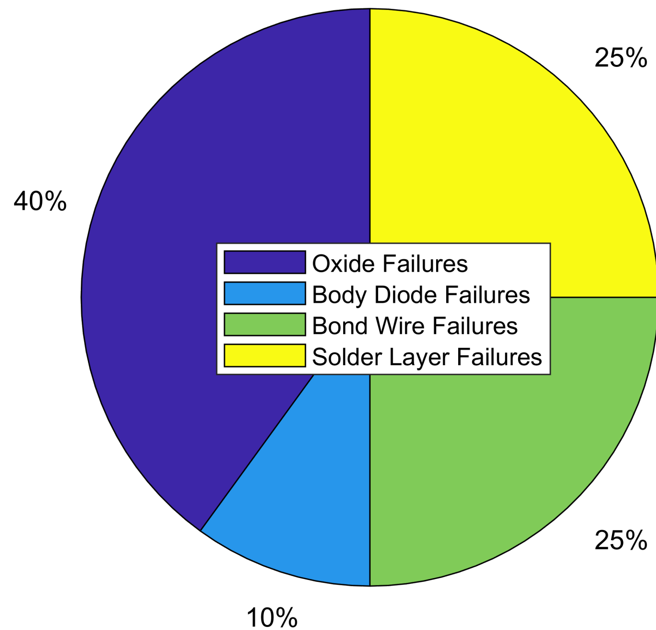

Figure 2.3: Failures type reviewed papers proportion[11]

Paradoxical,the failure analysis of MOSFET is young and old research topics and a lot of researches are carried out every year and Figure 2.3 shows the proportion or ratio of the number of papers reviewed for the different type of failures.

2.2 Active Thermal Control Strategies, ATC

Active thermal control is a temperature cyclic stress management strategy or control mechanism for power semiconductor devices with the help of control parameter adjustment or adding an external coolant part. Those ATC strategies are classified into different perspectives. This thesis classifies ATC into three broad categories load and switching control, cooling and external management, and finally, feedback and sensing control groups. Each of the three groups is classified into hardware-based and software-based. Due to the hardware types taking extra space, cost, and mechanical compatibility problems, this thesis focuses on software types.

2.2.1 Load and switching control

Load current control is one of the active control strategies for junction temperature management. Load current has a direct impact on power losses, especially conduction losses. Active control of load current through different techniques such as pulse-width modulation (PWM), current limiting, modulation index or duty cycle of

Table 2.1: Failure and Characteristics summery in Power Electronic Devices [11]

Failures Type	**Failure's Location**	**Failure Cause**	**Failures Result**	**Reference Parameters**
Gate Oxide	Gate oxide	High electric field, high temperature	TDDB, avalanche breakdown, short circuit	Gate leakage current, threshold voltage, drain leakage current, Miller plateau
Body Diode	diode body	Forward bias	Stacking fault, open circuit	Drain-leakage current, forward voltage
Bond Wire	bond wire	Thermo mechanical stress	Bond wire lift-off, bond wire fractures	On-state voltage, on-state resistance, bond wire resistance
Solder Layer	solder layer	Thermo mechanical stress	Crack and void	Solder-layer resistance, junction-to-case thermal resistance

the switching signal can effectively reduce conduction losses and can be kept within acceptable limits that mitigating power losses.

The controller's function in load current management is emphasized in the study "Optimal Control of Traction Motor Drives Under electro-thermal Constraints" by Lemmens et al. The system controls the switching frequency and current by including temperature feedback with real-time estimates [46] .The load current control model is also implemented in a micro-controller. That is essential for actual world monitoring , handling and ensures regulated thermal performance in power semiconductor devices [47].The microprocessor is extra hardware and causes extra cost, complexity and power loss.

Load Current-Based Gate Voltage Control: Using a load current feedback controller, the different parameters of the converter can be controlled, such as the gate voltage.This system requires proper reference of the load current and uses a robust proportional integral controller controls load current and provides reference gate voltage. While these control strategies provides plenty benefits in terms of reliability, efficiency, and component lifespan, it also come with drawbacks related to complexity, cost, and trade-offs that need to be carefully considered during the

Table 2.2: Classification of ATC [10]

ATC		
Load and switching control	**Cooling and external control**	**Feedback and sensing control**
Hardware Based	**Hardware Based**	**Hardware Based**
• Switching Transient Control – Duty Cycle Reduction Techniques – Gate Resistance Manipulation – Gate Voltage Manipulation – Step-Wise Gate Driver – Turn-Off Delay Control • Active Shoot-through	• Fan • Magneto hydrodynamic • Balancing thermal stress with topology – parallel connected – series connected	• Virtual Heat Sink
Software Based	**Software Based**	**Software Based**
• Load Current Control – Load Current Based Gate Voltage Control – Load Current Based Switching Frequency Control – Region Based Load Current Active Thermal Control • Frequency Control – CPWM – DPWM • Modulation Index and Power Factor	• -	• Junction Temperature • Switching Power Loss • Conduction Power Loss

design and implementation of power converters [48].

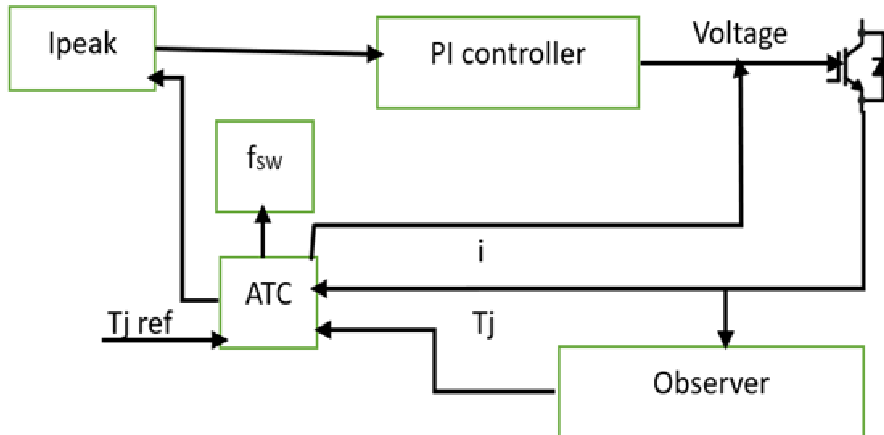

Figure 2.4: Load current control for desired voltage reference [48]

Load Current Based Switching Frequency Control:using filed oriented control ,FOC of the load current control in electric vehicle application, it is possible to get good result of junction temperature management by adjusting the switching frequency as the load current input determines the hysteresis controller.The controller monitors the temperate as when higher load is there increase the frequency and for low load decrease the frequency [51].Therefore the switching frequency is increased and decreased based on the load level but this way of control reduce the system performance.

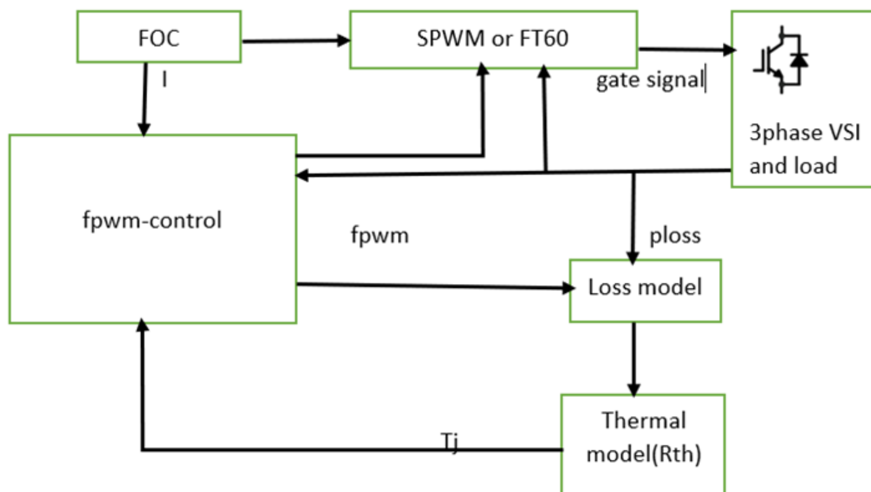

Figure 2.5: Load current based frequency control [49]

Region-Based Load Current Active Thermal Control: To prevent overheating and power cycle failures some active thermal management of power electronic modules uses a region-based control .Which is carefully engineered to control

both mean temperature and temperature swing. It separates the operational spectrum into discrete thermal areas, each designating a particular operating mode: regular operation, overheating, shutdown, power cycling high, and power cycling low [52].Even if the region-based controller for active thermal control offers essential advantages in terms of handling thermal stress, it also comes with challenges related to complexity and computational overhead. Careful design and implementation are necessary to utilize this controller's advantages fully [53].

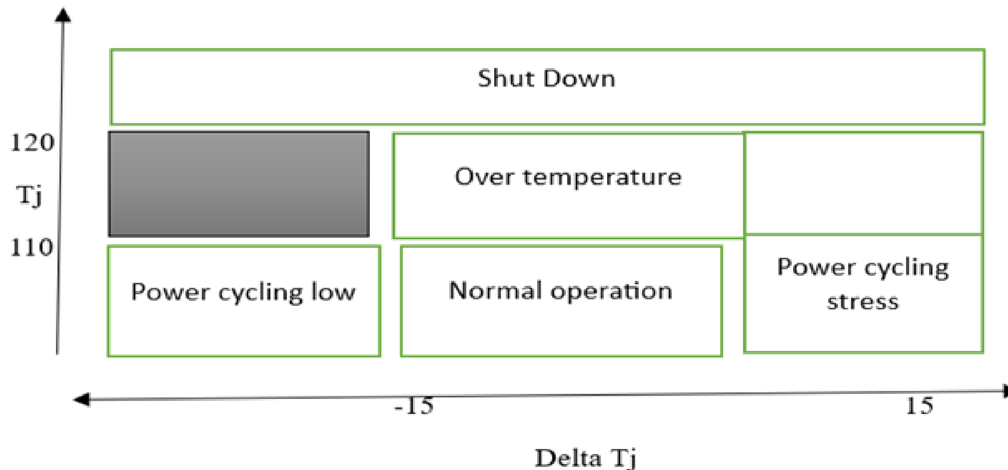

Figure 2.6: Region definition for different temperature profile [53]

Frequency Control: Frequency control plays a significant role in power semiconductors because it dramatically impacts switching losses. Frequency control techniques can minimize power loss by dynamically altering the switching frequency in response to temperature feedback and load circumstances [54]. High switching frequency increases the switching loss but reduces conduction loss. At the same time, a lower switching frequency provides lower switching loss but higher conduction loss. The switching frequency can be indirectly controlled by modulation index, power factor, or any other plant speed parameter once the junction temperature change has been detected [54].

$$f_{\text{sw}} = \begin{cases} f_{\text{sw_max}} & \text{for low junction temperature,} \\ f_{\text{sw_min}} & \text{for high junction temperature,} \\ f_{\text{sw}} & \text{for junction temperature within limit.} \end{cases} \tag{2.1}$$

Discontinuous PWM(DPWM) is also another frequency control strategy with a different modulation technique that modifies the power device switching patterns to lower switching losses and increase efficiency. In comparesion with conventional PWM methods, DPWM purposefully or intentionally creates brief intervals or pause during which the switching process is stopped for a moment. Resulting in discrete or discontinuous current waveform. This provides modifying the switching pattern in response to temperature feedback received in real-time from the devices or the external environment [55]. While different research uses sinusoidal PWM technique and

flat top 60 modulation techniques, this thesis uses the usual PWM techniques. This methods is robust and well-established, reduce computational burden and provide simplicity, high efficiency, and, most importantly, broad compatibility, ensuring their applicability in a wide range of scenarios [49]. But Discontinuous PWM(DPWM) are good for specific application such as needs high accuracy and high efficiency .

Modulation Index and Power Factor: As power factor decrease which indicates higher reactive power circulating and so the flow of current increase.This lost power increase and vice-versa. It is required using proper power factor correction techniques to reduce the phase difference between voltage and current. Modulation index directly related with switching frequency and duty cycle and affects both conduction and switching loss.Load current directly impacts junction temperature since more significant currents cause semiconductor devices to heat up and dissipate more energy. The power delivered to the load can be precisely adjusted thanks to the increased precision of the control overload current with flat-top PWM. When compared to conventional PWM methods, the advantages of 60° flat top PWM include decreased harmonic distortion, increased efficiency, and smoother motor running. However, more intricate control algorithms and circuitry could be needed to execute it successfully [49].

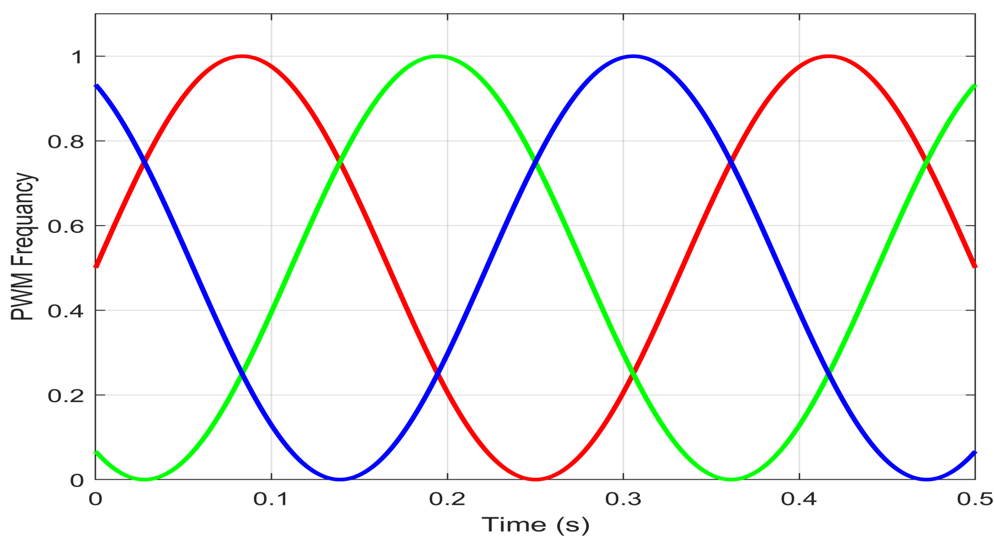

Figure 2.7: Sinusoidal PWM signal

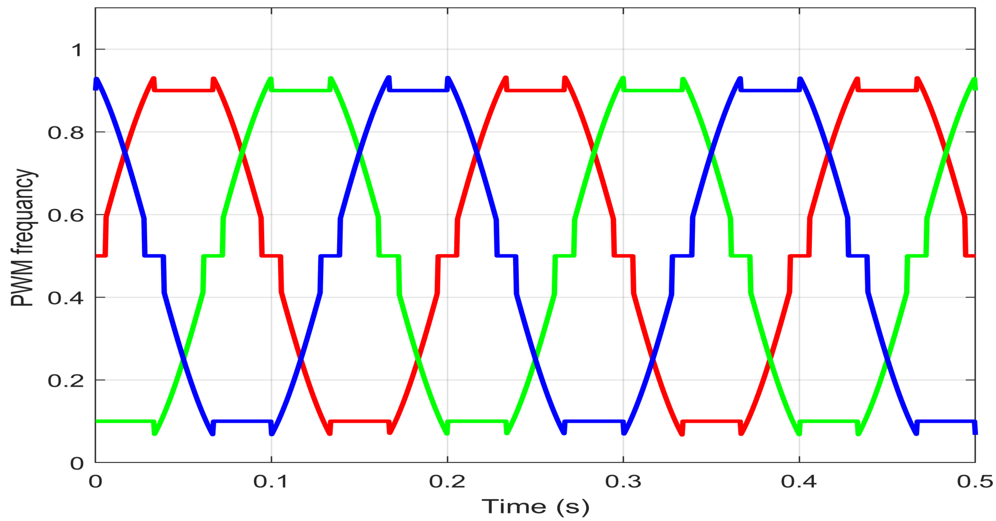

Figure 2.8: Flat top 60 PWM signal

Some techniques may use a look-up table and junction temperature feedback from the loss analytics model, together with frequency hysteresis control. This method starts by setting the command switching frequency and adjusting it based on the loss and junction temperature, especially for drive applications [57].

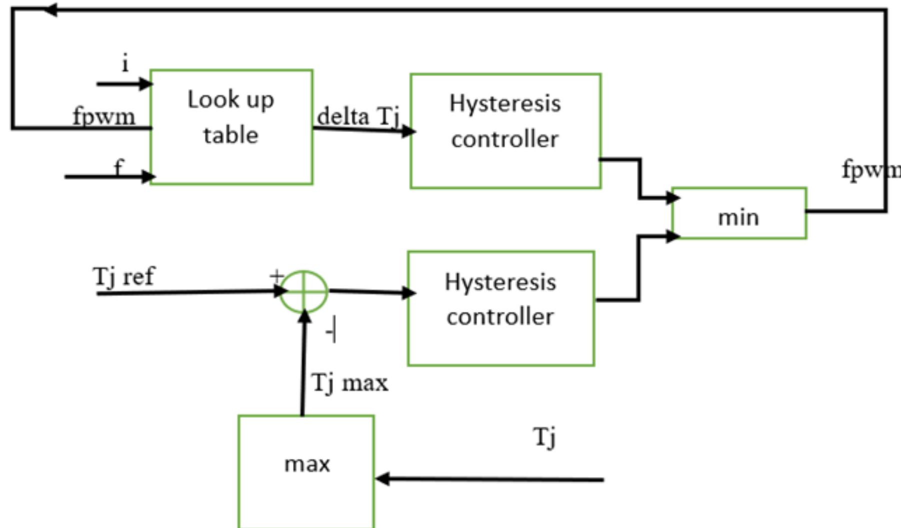

Figure 2.9: Hysteresis frequency controller [49]

Duty Cycle Reduction Techniques: Transitions between switches are a key places where potential power losses happened. Switching losses can be reduced by optimizing switching transients using sophisticated control algorithms and circuit design strategies like zero-voltage switching (ZVS) or zero-current switching (ZCS) [11]. By minimizing the overlap of the voltage and current waveforms during switching events, these solutions seek to decrease the rise in junction temperature and mitigate power losses [11] .This techniques requires additional sunnaber circuit

Table 2.3: Classification of Hhardware ATC [10]

Hardware ATC	
Load and Switching Control	**Working Principle**
- Gate Resistance Manipulation	Adjusts the gate resistance to control the switching speed and thermal stress[61].
- Gate Voltage Manipulation	Modifies gate voltage to control switching dynamics and reduce power loss[62].
- Step-Wise Gate Driver	Provides gradual gate voltage changes to control switching losses[60].
- Turn-Off Delay Control	Delays the turn-off process to reduce voltage spikes and thermal stress[64].
- Active Shoot-through	Introduces intentional shoot-through to balance thermal stress across devices[65].
-Duty Cycle Reduction Techniques	Reduces the on-time of switches to limit heat generation[11].
Cooling and External Control	
- Fan	Provides active cooling by forcing air over the heat sinks[67].
- Magneto hydrodynamic	Uses magnetic fields and electrically conducting fluids for cooling[69].
- Balancing Thermal Stress with Topology	Distributes current or voltage to reduce stress in parallel or series configurations[68].
Feedback and Sensing Control	
- Virtual Heat Sink	Simulates additional cooling capacity through advanced control algorithms that optimize thermal performance[61].

and sometime provides reduced system performance.

The average power applied to the load is directly impacted by the duty cycle of a PWM signal. The average power dissipation in semiconductor devices falls propor-

tionately with a reduced duty cycle [59]. The devices produce less heat as a result of this drop in power dissipation, which lowers the junction temperatures of the devices. The control approach entails modifying the converter's duty cycle in response to system feedback. Measurements of temperature, current, voltage, or other characteristics may be included in this feedback. Switching losses happen when power electronic devices like MOSFETs or IGBTs switch from an ON to an OFF state and vice versa. The duty cycle of the PWM signal affects both the switching frequency and the switching timings, which are proportionate to these losses. Lower switching losses usually result from a decrease in the switching frequency caused by a reduction in the duty cycle. Consequently each switching cycle produces heat which lowers the junction temperature [59].

When semiconductors are in the ON state, conduction losses happen because of their resistance. The length of the ON state in relation to the entire switching period is determined by the PWM signal's duty cycle. Lower conduction losses result from a reduction in the duty cycle, which also shortens the semiconductor devices' ON time. As a result, less power escapes the devices as heat, which lessens the impact of the rising junction temperature. Thus, a helpful way to regulate junction temperature in power electronic systems is to lower the duty cycle in a PWM control scheme [60].

Gate resistance manipulation techniques: different resistance based management such as adaptive gate driver, gate resistance selection circuit and gate resistance adjustment algorithms are used to reduce loss and thermal stress in power electronic converters. This is done by fast or slow charging speed of the gate capacitance. Therefore, the time spent for the gate voltage to reach the threshold level increases or decreases and so the switching processes are controlled based on this resistance. This can be implemented using a galvanically isolated DC/DC power supply, together with linear regulator, and complex programmable logic device [61].

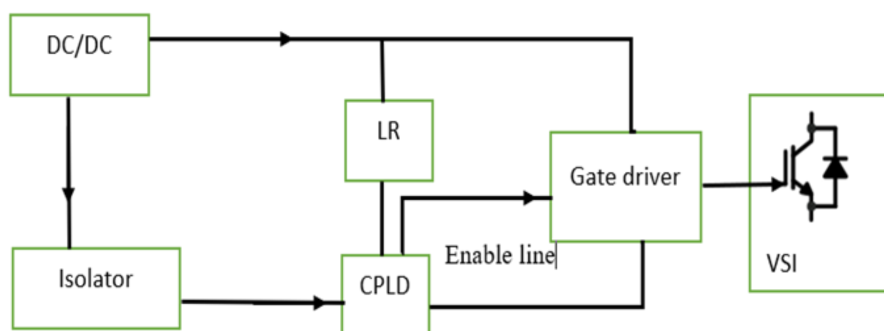

Figure 2.10: Adaptive IGBT gate drivers [61]

Gate resistance control method is often combined with PWM frequency adjustment to enhance the overall loss manipulation range and optimize thermal control [61].

Step-Wies gate driver and Gate voltage manipulation: These active gate controls can also be used to lessen semiconductor heat cycling by changing the control parameters such as on time. It is possible to reduce thermal cycling by

adjusting the gate drive voltage since it affects the semiconductors' conduction and switching losses. [60].

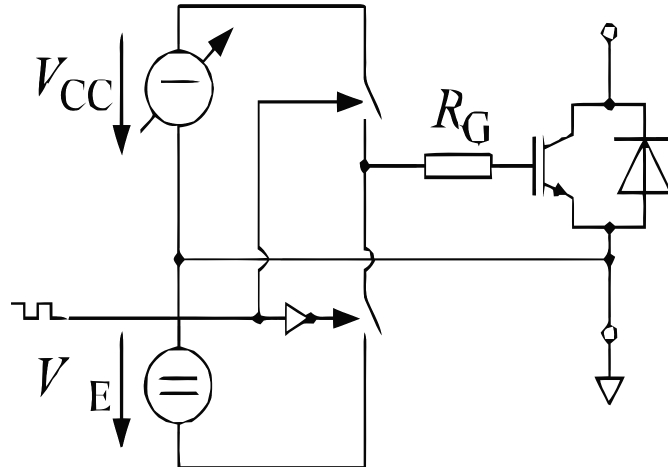

Figure 2.11: Gate voltage control active control mechanism [60]

Gate voltage monitoring reshape wave form's, length and magnitude of gate voltage to maximize switching performance [62]. It provides a discrete type of wave form instead of continuous voltage waveform. The special gate driver generates a series of voltage steps with predetermined magnitudes and duration's. Step wise gate drivers offer precise control over voltage and current waveform during switching transitions and this reduces extra voltage and current stress over components.This is accomplished by accelerating switching speed, cutting down on time in high-loss areas and applying a quick and regulated voltage ramp during transitions. By regulating the voltage change rate, step wise gate driver switching lowers switching losses and power device thermal cycling. This improves device reliability and lessens mechanical stress with additional cost and complexity from the traditional gate driver [62].

Turn-off delay control: This is a method for actively controlling the junction temperature of IGBTs or MOSFET power semiconductors by monitoring the turn-off transition time delay. The method involves shifting the IGBT's turn-off trajectory to adjust its turn-off loss. When the load decreases, the average load current decreases, so the junction temperature decreases and creates temperature swings. Therefore in order to maintain the junction temperature constant, it is required to hold the loss with specific defined region . So ,during low load condition the transition delay time should be extended to increase the loss and this have the junction temperature constant and smooth [64].

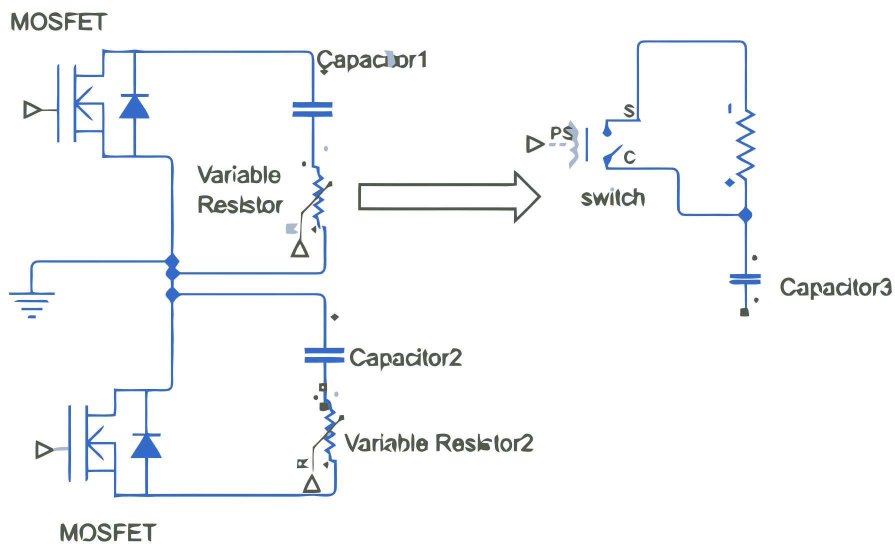

Figure 2.12: Turn-off trajectory adjustment circuit (TTAC) [64]

Active Shoot-through: A controlled Shoot-through system can monitor the temperature and load levels of power devices [65].This Active Thermal Control (ATC) mechanism is functioned when the system senses low load conditions, which means that the equipment is not functioning at its maximum performance. Controlled shoot-through happens when there is little load, simultaneously turning on the high-side and low-side switches in a half-bridge topology.By purposefully overlapping the power devices, the devices self-heat to maintain a more uniform temperature and this lowering stress and thermal cycles. This active shoot-through model works only for low load conditions by increasing the power loss to maintain the temperature constant. It does not work for high load conditions, and it also needs extra hardware and reduces efficiency.

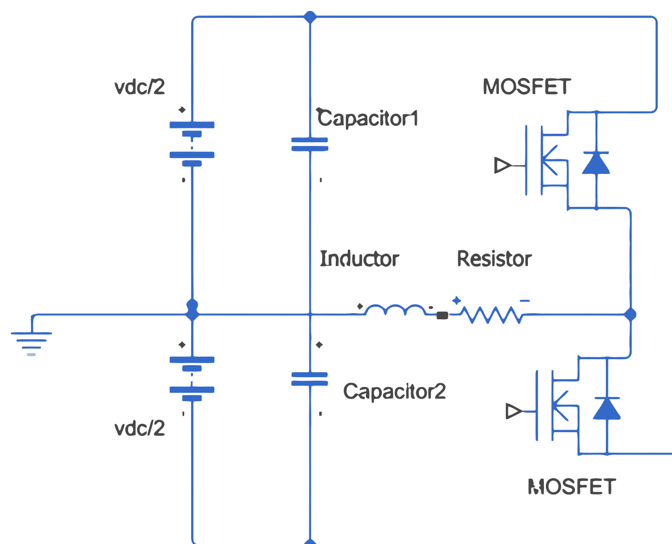

Figure 2.13: Schematic of half-bridge converter with split DC supply [65]

2.2.2 Active Cooling Mechanisms (fan and magnetohydrodynamic)

Most of the active cooling strategies are the hardware type of active thermal controls. This thesis basically grouped in to fan, Magnetohydrodynamic and topology management strategies.Fan speed is increased or decreased by feedback junction temperature reading using Temperature sensors such as thermocouples are positioned in easily accessible areas of the power electronic module to detect temperature. Analog-to-digital converters (ADC) are used to transform analog temperature measurements from the sensors into digital signals that the digital signal processor (DSP) can analyze. The state observer algorithm processes the temperature readings and system dynamics to estimate the temperature at critical points within the power module [67].

Magnetohydrodynamic (MHD) is a liquid used as active control mechansim. Liquid metal is used as the coolant due to its high thermal conductivity compared to traditional coolants like water and other oils. This magnetohydrodynamics method requires sophisticated control mechanism such as detecting the magnetic filed and relating to the temperature cyclic stress. It is a metal liquid that controls the junction temperature by flowing around the high temprature region .It removes heat from the module. The liquied flow reat is activly controlled based the the junction temprature feedback sigal from sensor or observer.This enables proactive thermal management by offsetting temperature variations and reducing thermal cycles caused by load changes. The system sometime incorporates an adaptive heat sink that adjusts cooling performance to offset temperature variations. This helps reduce the module's fatigue and increases the lifetime of power semiconductor devices. Traditional cooling methods like forced air/liquid cooling, heat pipes, and synthetic jets have limitations such as large size, slow response time, and inconvenient temperature control and needs more sophisticated and adaptable control mechanism [69].

2.2.3 Sensing and Feedback Control

The feedback and sensing control mechanism uses the junction temperature as a feedback reference to adjust the the switching or conduction loss. Virtual heat sink is another feedback control mechanism.The junction temperature is estimated by two different ways , using sensor [49, 57] and using online estimator algorithm without using sensor and no extra hardware change over the system [58] .The later one reduces the system complexity and also cost but provide good result like that uses sensor.
This thesis manages the switching loss using hysteresis control strategies so the junction temperatures remain within the defined region.Virtual heat sink is another feedback control mechanism [61].

2.2.4 Software Based ATC summery

As discussed by the above section, active thermal control are classified as load current control, junction temperature control, switching transient parameter like gate

resistance and gate voltage control and finally grouped as frequency control. That classification can be broadly grouped into hardware-based and software-based active thermal control. Software-based ATC strategies are more advantageous than the hardware type since they reduce cost, increase energy density, and play a role in the compactness of the inverter. The software groups are described briefly below in table form as classified in three major group in load current, PWM frequency control and discontinuous PWM frequency control techniques and some use both range of junction temperature change and actual average junction temperature and some others uses only one of them.This ATC system is subdivided in to three as PWM frequency manipulation, load current manipulation and discontinuous PWM modulation techniques. Table 2.4- 2.6 shows the different categories of software based ATC strategies.

Table 2.4: PWM frequency based Software ATC strategies

Method (Working principle)	**Key experiment outcome**	**Advantage**	**Controller Input parameters**	**Application and Topology**
Controller: uses PI and region-based PI controller-uses observer				
Control switching loss by adjusting the PWM frequency, use sensor [71] and observer [53]	Regulate the thermal stress effectively	adaptive thermal management and enhanced reliability	Uses average and range of junction temperature	traction application, 2-level
Control switching loss by adjusting the PWM frequency using thermal observer and virtual heat sink [51]	Reduce thermal cycle more than 20%	broader range of loss manipulation allows for more precise control	Uses average and range of junction temperature	renewable energy system for 2-level
Controller: Uses hysteresis controller and no observer				
Control switching loss by adjusting the PWM frequency using the lookup table of manufacturer and online calculated power loss [60,72]	Smooth transition >15% and improve lifetime by >263%	Dynamically adjust the switching frequency	Uses average and range of junction temperature	Traction application 2-level voltage

Continued on next page

Table 2.4 – continued from previous page

Method (Working principle)	**Key experiment outcome**	**Advantage**	**Controller Input parameters**	**Application and Topology**
Control power loss by comparing the difference between actual loss and low pass filtered loss [73]	Thermal cycle reduced by 30%	Don't need junction temperature estimation	Uses range of junction temperature	-
Using the change in junction temperature, adjust the switching frequency [58,59]	extend lifetime but not quantified	Reduce excessive cooling down of IGBT by continuous junction temp checkup	Uses range of junction temperature	Traction application, 2-level

Table 2.4 describes the active thermal control strategies with PWM frequency manipulation,uses different controller types such as PI,hysteresis and fuzzy with and without junction temperature observer.

Table 2.5: Load current based Software ATC strategies

Method (Working principle)	**Key experiment outcome**	**Advantage**	**Controller Input parameters**	**Application and Topology**
Controller: Uses hysteresis controller and 60 use T_j observer				
Control switching loss by adjusting the load current by using the lookup table of manufacturer and online calculated power loss[60,72]	Smooth transition >15%	Dynamically adjust the switching load current	Uses average and range of junction temperature	Traction application 2-level voltage

Continued on next page

Table 2.5 – continued from previous page

Method (Working principle)	Key experiment outcome	Advantage	Controller Input parameters	Application and Topology
Using thermal observer estimate the junction temperature and ATC generate reference load current [49]	-	The technique can be customized and optimized for different applications	Uses average junction temperature	traction application ,2-level
Controller: undefined controller and no observer				
Optimizing the MPPT algorithm to minimize thermal stress, by restricting the positive temperature gradient and maximum junction temperature[74]	lifetime increased by 13%	Reduce thermal stress during fast-changing irradiance	Uses average and range of junction temperature	Photovoltaic power generation, 2-Level
ATC reduce temperature swing during low load by increasing conduction loss [75]	Reduce temperature swing	Improved reliability and lifetime	Uses average junction temperature	for traction application PMSM ,2-level

Table 2.5 describes the active thermal control strategies with load current manipulation,uses different controller types such as PI and hysteresis with and without junction temperature observer.

Table 2.6: DPWM frequency based Software ATC strategies

Method (Working principle)	**Key experiment outcome**	**Advantage**	**Controller Input parameters**	**Application and Topology**
Controller: Undefined controller and no observer				
Manipulating the switching losses by discontinuous pulse width modulation using clamping angle as control parameter[76]	71% power loss reduction by using 60 degree clamping angle	Reduce thermal stress very much	Uses average junction temperature	Renewable energy wind farm ,2-level
Techniques to reduce switching loss by Hybrid of (SVPWM) and (DPWM) [77]	Lifetime improved IGBT by 17% and diode by 8%	Reduced Thermal Stress	Uses average junction temperature	Electric Vehicles, PMSM ,2-level
Controller: Hysteresis controller and Tj approximation				
Adjust loss using discontinuous 60°-Flat-Top modulation (FT60) instead of sinusoidal modulation (SPWM) [50,578]	-	Reduce stress and improve lifetime	Uses average and range of junction temperature	Electric Vehicles, PMSM ,2-level
Controller: Finite control set with model predictive controller				
techniques to reduce switching loss by optimizing lifetime and switching speed using FCS-MPC [79,80]	Thermal overshoot reduced by 40%	Extend lifetime of IGBT and Reduced Thermal Stress	Uses average and range of junction temperature	Electric Vehicles, PMSM ,2-level

Table 2.6 describes the the active thermal control strategies with discontinues PWM modulation manipulation,uses different controller types such as model predictive and hysteresis with and without junction temperature observer.

3

System Modeling for ATC

The system model contains four components: the drive cycle in transient and cruise, the 1-D vehicle model, the machine model, and finally, the inverter analytic model with its hysteresis controller. Each model is described below, with more concern for the inverter analytic model and, finally, verification and parameter analysis.

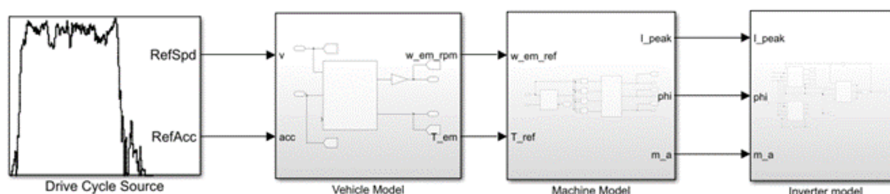

Figure 3.1: System model in block diagram

3.1 Analytical Power Loss Calculation

Some of the applications such as electromobility, solar and wind energy systems, and much industrial automation are a few applications that depend on power electronic equipment. Controlling power outages of these power electronics is very essential and considering the increasing demand for efficiency and reliability. These power loss affects junction temperature which plays a significant role in lifetime and reliability.High junction temperatures can speed up the aging process of the electrical equipment and this may leads to a catastrophic failure. To solve these issues, active thermal control strategies that lower junction temperature have been devised, and this thesis explored the effectiveness of several strategies in minimizing power loss by the previous chapter, considering switching and conduction losses together with their dependence on frequency control, load current, junction temperature and switching transients [1, 2].

Before discussing the ATC system used in this thesis, it is essential to model the power semiconductor device power losses. The loss is classified in to Conduction losses and switching losses as the two broad classification of power losses. Switching losses occurs when the switch transit between ON and OFF states. The switching frequency, different switching transient control strategies, and gate driver-can adjusted switching loss.To reduce switching losses in power converters, efficient switching strategies and designs are crucial and this thesis uses PWM frequency based ATC [1, 2, 80].

When a MOSFET starts transfer current due to the voltage drop on the ON-state resistance , conduction loss happens .Especially at high current levels conduction loss significantly determines the power converters overall efficiency . Reducing conduction losses in power electronic systems requires careful consideration of design factors minimizing ON-state resistance, power factor, modulation index, and load current, which also contribute to conduction losses and have a more significant potential to impact the loss negatively [1, 2, 4].

The switch turn on and off quickly in high rate of frequency applications are more likely to experience switching loss. increasing switching frequencies may result in increase switching losses, affects the system efficacy. System performance can be improved and switching losses can be decreased using desired strategies . Also the conduction loss typically has a greater impact on applications that need high current levels and continuous operation.Therefore, the actual impact of switching loss and conduction loss on power semiconductors devices depends on factors such as operating frequency, current levels, duty cycle, and thermal handling strategies and careful consideration of both types of losses and optimize the system to minimize overall power dissipation and maximize efficiency [1–4]. It is enough to examine the single legs of the three-phase inverter, and the remaining five legs follow the same procedure, and the power loss of one leg of the converter is one-sixth of the total converter and described as below in equation 3.1.

$$P_{\text{tot_loss}} = P_{\text{sw_loss}} + P_{\text{cond_loss}} \tag{3.1}$$

Where $P_{\text{tot_loss}}$ is the total power loss, $P_{\text{sw_loss}}$ is the switching loss, and $P_{\text{cond_loss}}$ is the conduction loss.
As shown in equation 3.1,the combined effect of switching and conduction losses provides the total power loss. This relationship is crucial for understanding the thermal and efficiency characteristics of power electronic systems.

3.1.1 Switching loss

When the switch starts to turn on and off, the switching loss occurs. Turn-on loss energy lost during the device's turn-on transition and Turn-off loss energy lost during the device's turnoff transition are the two primary components of switching loss beside with a small revers recovery power loss. Variations in voltage and current levels, as well as the features of the semiconductor device itself, are the causes of switching. The turn-on and turnoff switching frequency plays a big role in switching loss. Therefore, this thesis uses energy lost during turn-on and turnoff with switching frequency to model the switching loss as equation 3.2 [4].

$$P_{\text{sw_loss}} = f_{\text{sw}} \left(E_{\text{on-Idc}} + E_{\text{off-Idc}} + E_{\text{rr-Idc}} \right) \tag{3.2}$$

Where:

- f_{sw} is the switching frequency,
- $E_{\text{on-Idc}}$ is the energy lost during the on transition with respect to the specific DC current,

- $E_{\text{off-Idc}}$ is the energy lost during the off transition with respect to the specific DC current,
- $E_{\text{rr-Idc}}$ is the reverse recovery energy lost with respect to the specific DC current.

The DC current is approximated by dividing the peak value of one of the three-phase load currents by π [4].

$$I_{\text{dc}} = \frac{I_{\text{peak}}}{\pi} \tag{3.3}$$

Where I_{dc} is the DC current and I_{peak} is the peak value of the single-phase load current.

The on-state and off-state energy losses need to be scaled according to the applied DC-link voltage and the power semiconductor's standard or experimentally verified reference value [4].

$$E_{\text{scale-Idc}} = \left(\frac{V_{\text{DS}}}{V_{\text{DC}}}\right)^{k_V} \tag{3.4}$$

Where $E_{\text{scale-Idc}}$ is a multiplying scale factor for both the on-state and off-state energy losses, V_{DS} is the actual provided DC link voltage, V_{DC} is the reference DC voltage value of the power semiconductor, and k_V is a constant approximately equal to 1.4 [4].

3.1.2 Conduction loss

The conduction loss includes reverse conduction, parallel conduction (both diode and switch of the MOSFET conduct simultaneously), and blanking time losses. The analytic model of this conduction loss uses load current, modulation index, power factor, and dc-link voltage parameters as input and on-state resistance, junction temperature blanking time, and thermal network resistance as model parameters [4]. Therefore, conduction loss is mathematically described by the equations 3.5,

$$\begin{aligned} P_{\text{cond_loss}} =& \frac{R_{\text{on}} I_{\text{peak}}^2}{4\pi}\left(p_1 p_2 + p_3 p_4\right) \\ &+ \frac{R_{\text{on}}}{4\pi(R_{\text{on}} + R_d)^2}\Big(I_{\text{peak}}^2 R_d^2 \left(p_1(\pi - p_2) - p_3 p_4\right) \\ &+ v_d^2(\pi - 2\beta)p_1 - p_4\cos(\beta)\Big) \\ &+ I_{\text{peak}} R_d v_d \left(4p_1\cos(\beta) - (\pi - p_2)p_4\right) \end{aligned} \tag{3.5}$$

Where:

- R_{on} represents the on-state resistance,
- R_d represents the diode resistance,
- v_d represents the diode forward threshold voltage,
- I_{peak} represents the peak value of the single-phase load current.

The parameters p_1, p_2, p_3, and p_4 are defined as equation 3.6-3.9

$$p_1 = \begin{cases} 1, & \text{for } t_{\text{bl}} = 0 \\ 1 - 2t_{\text{bl}} f_{\text{sw}}, & \text{for } t_{\text{bl}} > 0 \end{cases} \tag{3.6}$$

$$p_2 = \frac{\pi}{2} + \beta - \frac{\sin(2\beta)}{2} \tag{3.7}$$

$$p_3 = \cos(\beta) - \frac{\cos^3(\beta)}{3} \tag{3.8}$$

$$p_4 = 2M\cos(\phi) \tag{3.9}$$

where:

- t_{bl} represents the blanking time,
- ϕ represents the power factor angle,
- M represents the modulation index,
- β represents the parallel conduction angle, defined as equation 3.10:

$$\sin(\beta) = \frac{v_d}{R_{\text{on}} I_{\text{peak}}} \tag{3.10}$$

3.2 Junction Temperature Estimation and RC Thermal Network

Since the power is calculated for single legs of the converter from the total six legs ,the junction temperature T_j can be calculated using the total power loss and the thermal network resistance as:

$$T_j = P_{\text{tot_loss}} \cdot R_{\text{th}} + T_{\text{amb}} \tag{3.11}$$

where T_j represents the junction temperature,$P_{\text{tot_loss}}$ represents the total power loss,R_{th} represents the thermal network resistance,T_{amb} represents the ambient temperature.

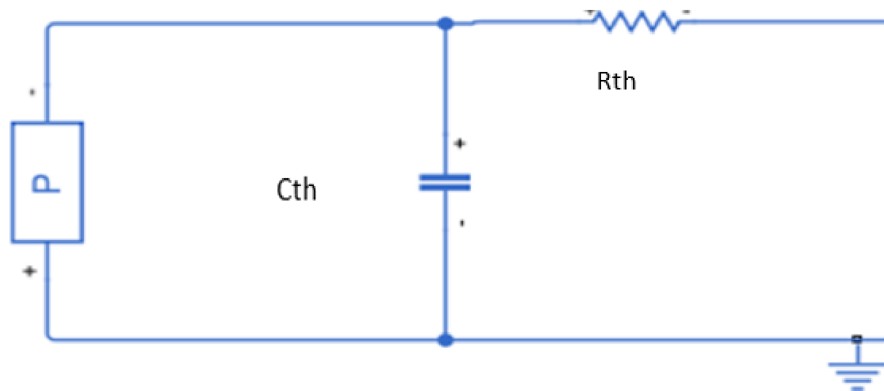

Figure 3.2: First-order (1-D) cauer type thermal network

There are two different type of junction thermal network model, cauer type and foster type.Cauer model represents the actual physical system and the foster model is simplified mathematical representation of the thermal response .Therefore for more accurate real world representation , this thesis use cauer type of thermal network.

The thermal network is modeled using a first-order RC network, which is represented in Figure 3.2.

$$t_r = \begin{cases} 2.2 \times \tau & \text{where } \tau = Rth \times Cth, \\ \frac{2.2}{\alpha} & \text{where } \tau = \frac{1}{\alpha}. \end{cases} \tag{3.12}$$

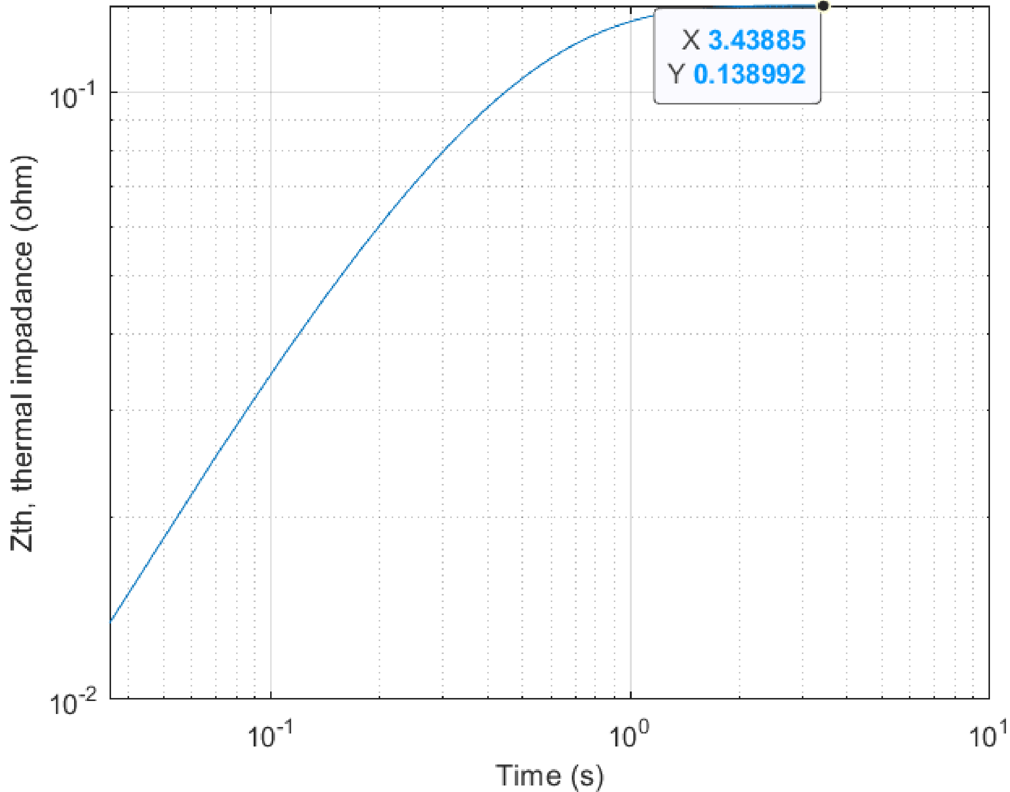

Figure 3.3: Thermal network impedance [6]

According to the thermal network data sheet from Hybridpack as shown in figure 3.3, the maximum thermal network impedance is 0.1389 ohm.The capacitance is calculated using the rise time of the thermal impedance figure 3.3 and time constant relation. According to the 10%-90% rise time calculation, the rise time is 0.7775 second.then using the equation 3.12,the capacitance value used is obtained as 2.35 Farads.

3.3 Rain Flow Counting

This thesis examines the effect of junction temperature by estimating the lifetime of power semiconductors.There are different method of lifetime estimation.
Monte Carlo Simulation and rainflow counting.However, this thesis uses rain flow counting method due to its accurate Representation of Real-World Loading Conditions,consistency with fatigue damage Models and efficient handling of complex

load histories . Especially in power electronics it is standard and widely accepted. Rain flow counting asses or estimates fatigue and stress by subdividing the loading history in to small scale.After subdividing, creates cycle with a pair of peaks and valleys based on the temperature loading or fatigue.Then by scanning the temperate data creates local maxima (peak) and local minima (valley) and analyze the cycle as the name implies rainflow using those peaks and valleys.Each cycle is classified or grouped based on the distance difference between the peak and valleys [82].

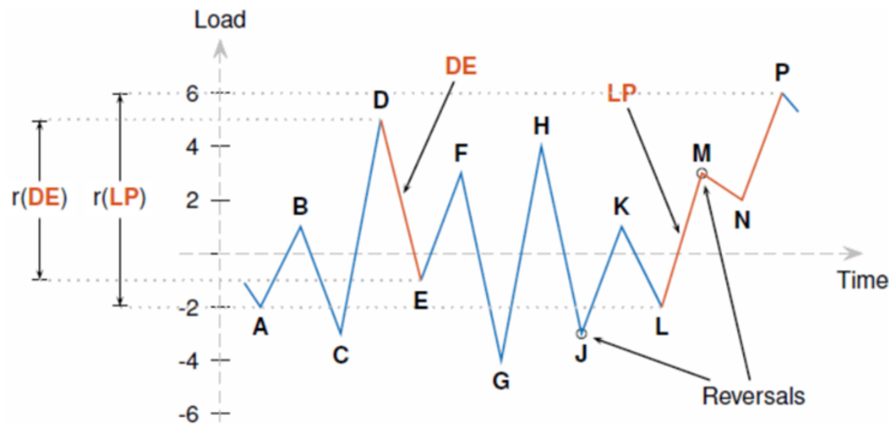

Figure 3.4: Rain flow counting principle [82]

The detail explanation of rain flow counting is not the objective of this thesis but in short description it starts the counting first by loading histories and identify reversal.As shown from figure 3.4, reversal is the turning point from high stress to low or from low stress to high stress.then by maintaining the reversal sequence arrange three point subset for two consecutive subset ranges.the next step is calculating the range Magnitude as shown in figure such as r(DE) and r(LP).Then calculate the cycle count using the cycle counting criteria [82].finally group the accumulated cycle for each amplitude or number of cycle at different amplitude.

3.4 Life Time Modeling

When it comes to SiC power converter lifetime prediction, data-driven models and Physics of Failure (PoF) models work well together and are frequently tasted by Accelerated Lifetime Testing (ALT). In order to provide estimation on long-term degradation or damage depending on load stress conditions, PoF models rely on an understanding and mathematical description of the physical properties of failure, such as solder fatigue and gate oxide breakdown. On the other hand, data-driven models provides reliability indicators such as Remaining Useful Life (RUL) based on previous stored data and sophisticated machine learning, allowing for habitual continuous maintenance and actual world monitoring. Both strategies rely heavily on accelerated lifetime test, which speeds up failure mechanisms under carefully monitored circumstances to produce data that improves model validation and accuracy and closes the performance gap between theoretical forecasts and actual results [11]. The total lifetime is calculated using equation 3.15 with the help of different lifetime

model.

$$\text{Lifetime_consumed} = \frac{\text{hist_counts}}{N_f} \tag{3.13}$$

where N_f represents the number of cycles to failure, and hist_counts represents the number of cycles at the same magnitude

$$\text{Total_Lifetime_consumed} = \sum \text{Lifetime_consumed} \tag{3.14}$$

where Lifetime_consumed is the lifetime consumed at each magnitude.

$$\text{Lifetime_hr} = \frac{\max(\text{time})}{\text{Total_Lifetime_consumed} \times 3600} \tag{3.15}$$

where max(time) is the total time duration and Total_Lifetime_consumed is the sum of all lifetime consumed.

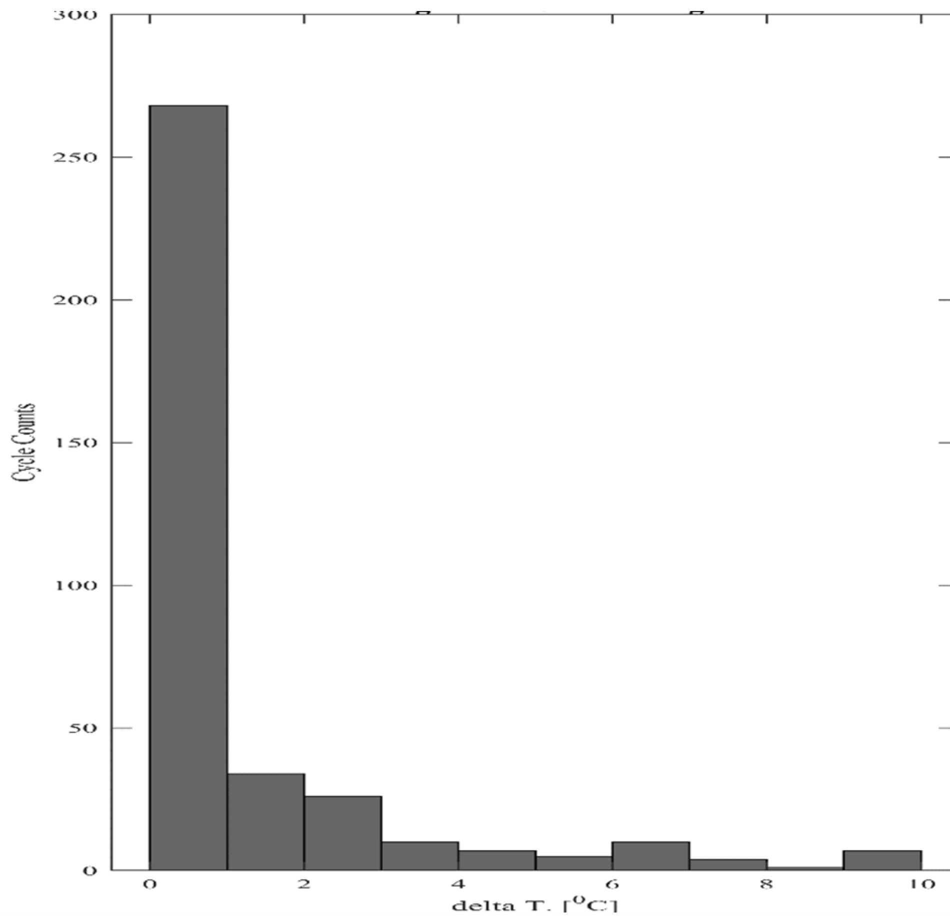

Figure 3.5: Histogram diagram with ten bins

The figure 3.5 shows the junction temperature and corresponding cycle to failures by grouping the cyclic stress in to ten bins.This rainflow histogram figure is generated based on the transient and Cruise drive cycle mode temperature load profile.Each cycle is comprehend with respect to number of failures to cycles(N_f).The total lifetime consumption is obtained from by adding all the cycle lifetime consumption.

In order to analyse the effect of junction temperature, this thesis uses different lifetime models for MOSFET (SiC) and IGBT(Si) power semiconductors from physics of Failure (PoF) Approach . Six-lifetime models, R. Bayerer et al. (CIPS 2008) for MOSFET and IGBT, the LESIT Project (1997) for IGBT solder layer fatigue and bond wire failures, and finally, the hybridpack model for SiC bond wire failure and solder layer fatigue, have used to analyze the effect of junction temperature and lifetime. All the models are described in terms of the number of cycles to failures with respect to a change in junction temperature, as shown below. The lifetime is done using rain flow counting techniques by grouping the similar range of junction temperature using histogram as the shown figure 3.5.

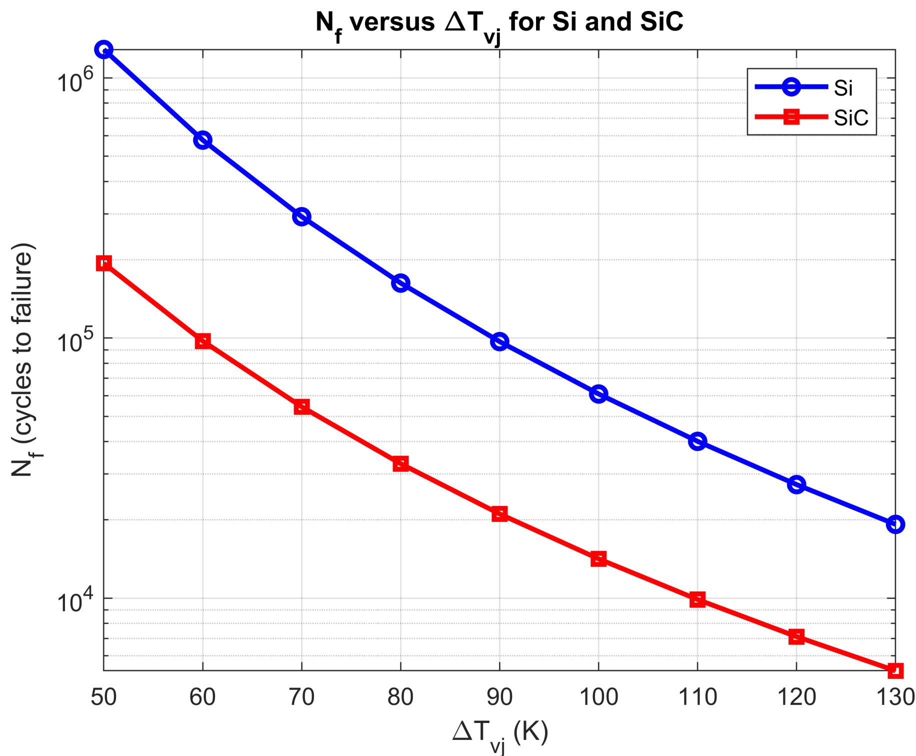

Figure 3.6: Si and SiC,R. Bayerer et al. (CIPS 2008) model [7]

Figure 3.6 shows the life time model of both Si and SiC designed by Bayerer and his colleagues during 2008.It is a general model of the power semiconductor ,doesn't specify specifically for solder layer and bond wire.The equation models below is lifetime of Silicon and silicon carbide power semiconductor devices based on temperature variations and current stress. The parameters account for the effects of operating conditions on the device's longevity.
The number of cycles to failure N_f for Silicon (Si) and SiC devices based on Bayerer et al. (CIPS 2008) is given by the following equation:

$$N_f = K'_{\mathrm{Si,SiC}} \cdot (\Delta T_j)^{\beta_{1,\mathrm{Si,SiC}}} \cdot \exp\left(\frac{\beta_{2,\mathrm{Si,SiC}}}{T_{\mathrm{vj_min_Si}}}\right) \cdot (I_{\mathrm{bw_Si,SiC}})^{\beta_{4,\mathrm{Si,SiC}}} \tag{3.16}$$

where:

- $K'_{\text{Si,SiC}} = \begin{cases} 3.19 \times 10^{12} & \text{for Si} \\ 1.31 \times 10^{10} & \text{for SiC} \end{cases}$: Material-specific constant.
- $\beta_{1,\text{Si,SiC}} = \begin{cases} -4.4 & \text{for Si} \\ -3.775 & \text{for SiC} \end{cases}$: Temperature dependence exponent.
- $\beta_{4,\text{Si,SiC}} = \begin{cases} -0.926 & \text{for Si} \\ -0.387 & \text{for SiC} \end{cases}$: Exponent for the current dependency.
- $T_{\text{vj_min_Si,SiC}} = 293$ K: Minimum junction temperature (calculated as $20 + 273$ K).
- $I_{\text{bw_Si,SiC}} = \frac{30}{4} = 7.5$ A: Current per bond wire.
- ΔT_j: Junction temperature swing.
- $\beta_{2,\text{Si,SiC}} = 1285$: Temperature coefficient affecting the lifetime.

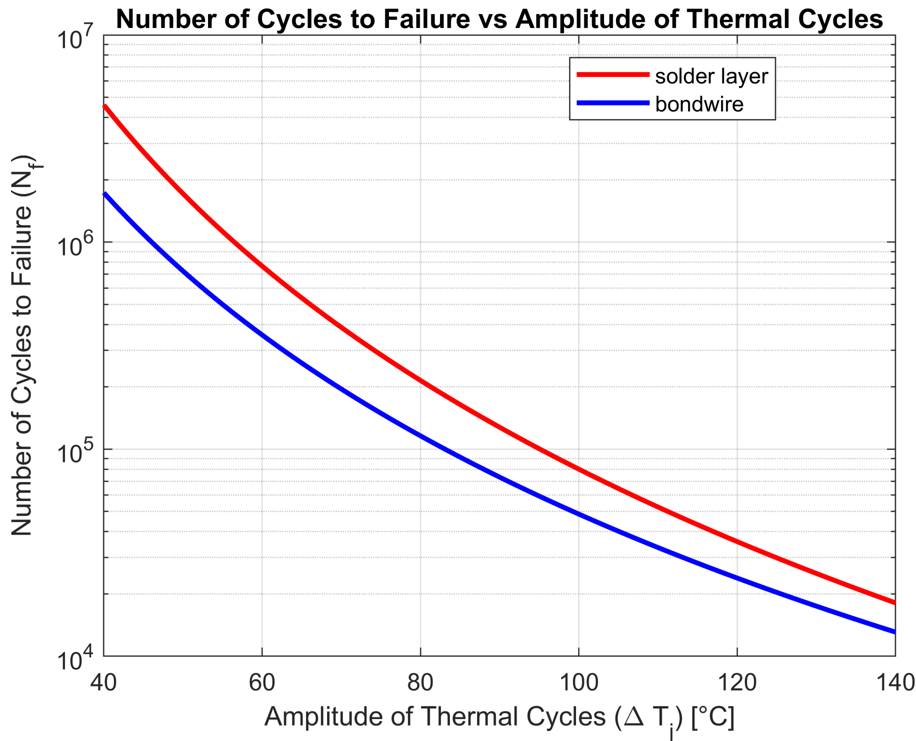

Figure 3.7: Si IGBT LESIT Project (1997) model [8]

Figure 3.7 shows the life time model of Si in solder layer and bond wire modeled by LESIT during 1997.The equation models below lifetime of Silicon power semiconductor devices based on temperature variations and current stress. The parameters account for the effects of operating conditions on the device's longevity.

$$N_f = \begin{cases} A_{\text{BW}} \cdot (\Delta T_j)^{\alpha_{\text{BW}}} \cdot \exp\left(\frac{E_{a,\text{BW}}}{k \cdot T_{\text{j_mean_K}}}\right) & \text{for bond wire (BW)} \\ A_{\text{SL}} \cdot (\Delta T_j)^{\alpha_{\text{SL}}} \cdot \exp\left(\frac{E_{a,\text{SL}}}{k \cdot T_{\text{j_mean_K}}}\right) & \text{for solder layer (SL)} \end{cases} \tag{3.17}$$

where:

- For Bond Wire (BW):

  - $A_{\mathrm{BW}} = 1.5 \times 10^{13}$: Pre-exponential factor.
  - $\alpha_{\mathrm{BW}} = -4.42$: Empirical constant.
  - $E_{a,\mathrm{BW}} = 0.0420$ eV: Activation energy.
- For Solder Layer (SL):
  - $A_{\mathrm{SL}} = 1.5 \times 10^{11}$: Pre-exponential factor.
  - $\alpha_{\mathrm{SL}} = -3.9$: Empirical constant.
  - $E_{a,\mathrm{SL}} = 0.0970$ eV: Activation energy.
- $k = 8.617 \times 10^{-5}$ eV/K: Boltzmann constant.
- $T_{\mathrm{j_mean_K}}$: Mean junction temperature in Kelvin.
- ΔT_j: Junction temperature swing.
- Mean junction temperature in Celsius $T_{\mathrm{j_mean}} = 100$ °C.
- Converted mean junction temperature in Kelvin $T_{\mathrm{j_mean_K}} = 373.15$ K (where $T_{\mathrm{j_mean_K}} = T_{\mathrm{j_mean}} + 273.15$).

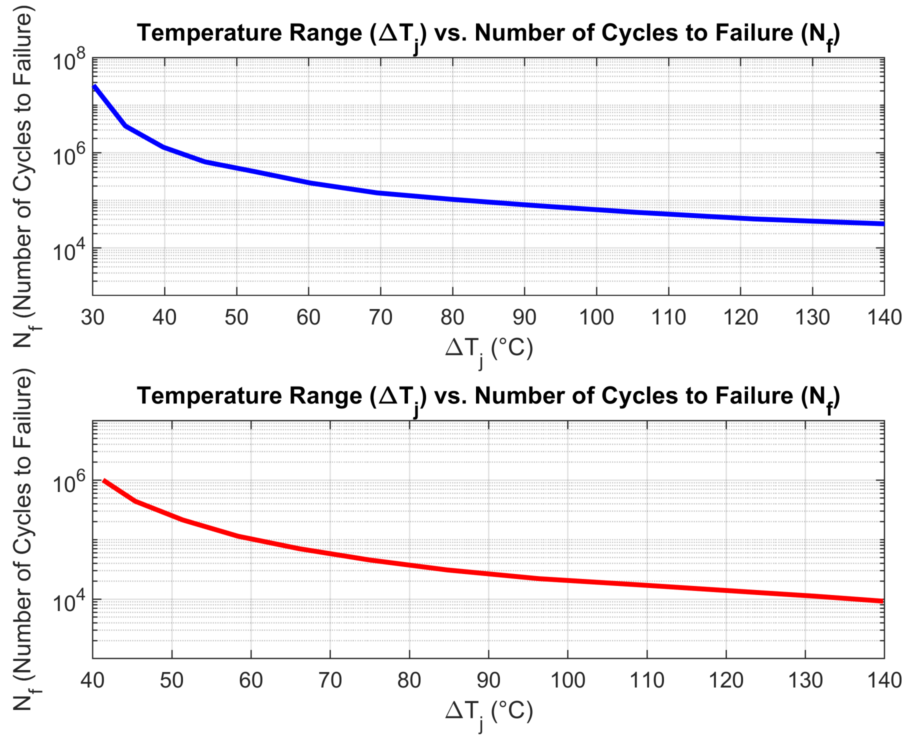

Figure 3.8: Hybridpack SiC life time model [9]

Figure 3.8 shows the life time model of SiC hybridpack power semiconductor in solder layer and bond wire modeled .The equation models below is lifetime of Silicon power semiconductor devices based on temperature variations and current stress. The parameters account for the effects of operating conditions on the device's longevity.

$$N_f = \begin{cases} A_{\mathrm{BW}} \cdot (\Delta T_j)^{\alpha_{\mathrm{BW}}} \cdot \exp\left(\frac{E_{a,\mathrm{BW}}}{k \cdot T_{\mathrm{j_mean_K}}}\right) & \text{for SiC bond wire (BW)} \\ A_{\mathrm{SL}} \cdot (\Delta T_j)^{\alpha_{\mathrm{SL}}} \cdot \exp\left(\frac{E_{a,\mathrm{SL}}}{k \cdot T_{\mathrm{j_mean_K}}}\right) & \text{for SiC solder layer (SL)} \end{cases} \tag{3.18}$$

where:

- For SiC Bond Wire (BW):
  - $A_{\text{BW}} = 1.00 \times 10^{13}$: Pre-exponential factor.
  - $\alpha_{\text{BW}} = -13.83$: Empirical constant.
  - $E_{a,\text{BW}} = 1.10$ eV: Activation energy.
  - $T_{\text{j_mean}} = 100$ °C: Mean junction temperature.
  - $T_{\text{j_mean_K}} = T_{\text{j_mean}} + 273.15 = 373.15$ K: Mean junction temperature in Kelvin.
  - ΔT_j: Junction temperature swing.
  - $k = 8.617 \times 10^{-5}$ eV/K: Boltzmann constant.
- For SiC Solder Layer (SL):
  - $A_{\text{SL}} = 1.00 \times 10^{13}$: Pre-exponential factor.
  - $\alpha_{\text{SL}} = -7.29$: Empirical constant.
  - $E_{a,\text{SL}} = 0.35$ eV: Activation energy.
  - $T_{\text{j_mean}} = 100$ °C: Mean junction temperature.
  - $T_{\text{j_mean_K}} = T_{\text{j_mean}} + 273.15 = 373.15$ K: Mean junction temperature in Kelvin.
  - ΔT_j: Junction temperature swing.
  - $k = 8.617 \times 10^{-5}$ eV/K: Boltzmann constant.

The life time result of those of each model are described by the next chapter by comparing with and without the controller.

3.5 Drive Cycle

The effect of the junction temperature is analysed for heavy heavy-duty diesel trucks (HHDDT) in combination with both transient and cruise modes of speed and acceleration for the 1-D vehicles.

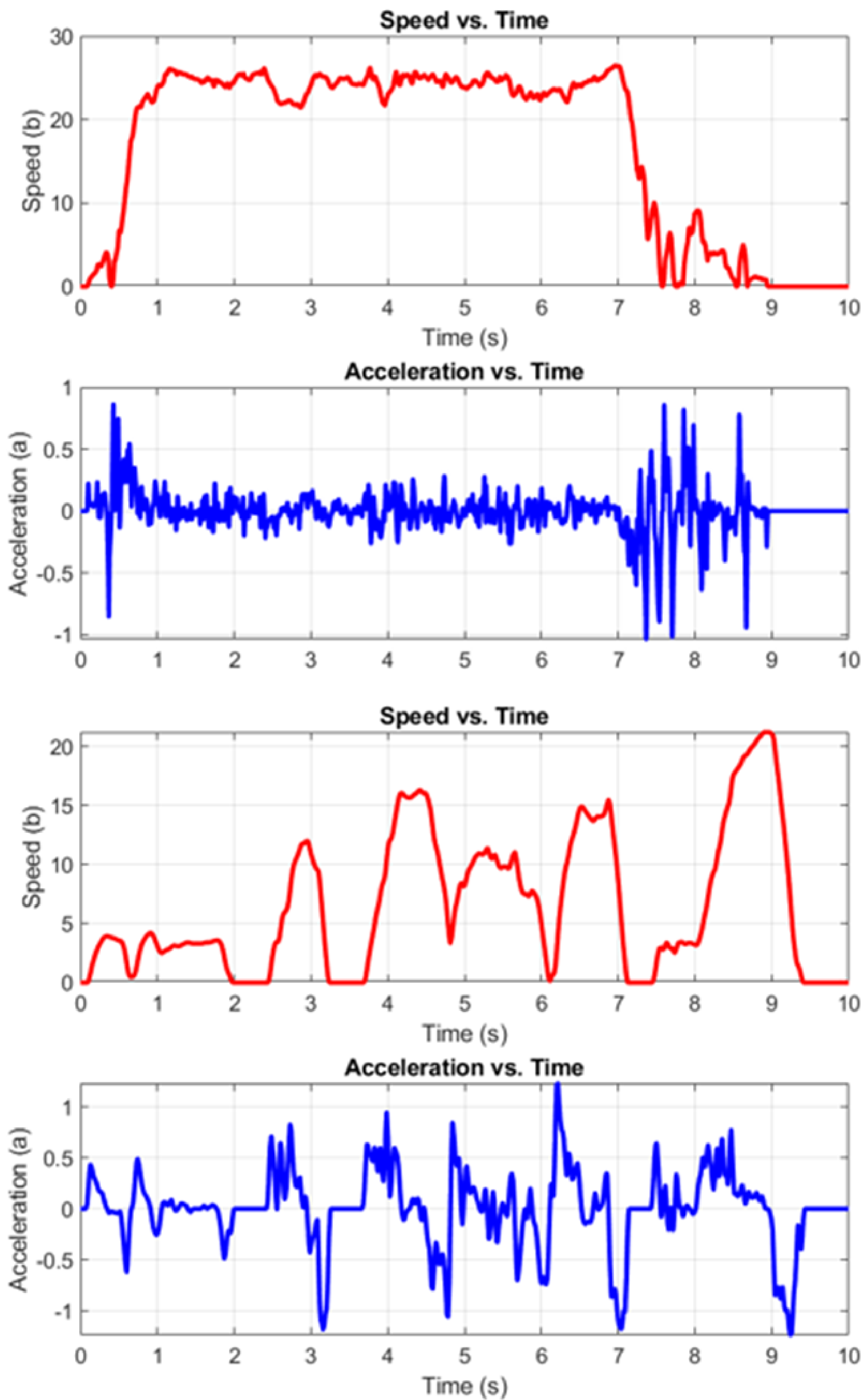

Figure 3.9: Cruise and transient reference speed and acceleration

the first two subplot shows the Cruise speed and acceleration and the last two

subplot shows the transient speed and acceleration. The Cruise mode shows very Little swing but the transient shows bit fluctuation.

3.6 Vehicle Model

Using Newton second law the vehicle is modelled using equation 3.19,the total force F acting on the vehicle can be expressed as [81]:

$$\sum F = m \cdot a = F_t - F_r = m \cdot \frac{dv}{dt} \tag{3.19}$$

where F represents the total force, m represents the mass of the vehicle, a represents the acceleration, F_t represents the total traction force,F_r represents the resistive force, v represents the velocity and the resistive force F_r is given by:

$$F_r = 0.5 \cdot \rho \cdot C_d \cdot A \cdot v^2 + m \cdot g \cdot \sin(\alpha) + m \cdot g \cdot C_r \tag{3.20}$$

where ρ represents the air density, C_d represents the aerodynamic drag coefficient,A represents the frontal area of the vehicle, v represents the velocity, g represents the acceleration due to gravity,α represents the road gradient,C_r represents the rolling resistance coefficient [81].

Using the reference speed and acceleration from the drive cycle, the electromagnetic torque T_{em} and the angular speed w_{em} are determined from the above 1-D vehicle model equation 3.19:

$$T_{\text{em}} = \frac{F_t \cdot w_r}{T_r \cdot n_{\text{em}}} \tag{3.21}$$

$$w_{\text{em}} = \frac{v}{w_r \cdot T_r} \tag{3.22}$$

where T_{em} is the electromagnetic torque, n_{em} is the number of drive units, w_r is the wheel ratio,T_r is the transmission ratio, w_{em} is the electromagnetic angular speed.

The following figure from figure 3.9 shows the drive cycle input speed and acceleration in transient and cruise drive modes.

3.7 Machine Model

In electrical machine for the purpose of simplification and easy analysis of the controller design it is mathematically described in quadrature and direct axis.the electrical circuit of each axis is shown below [83].

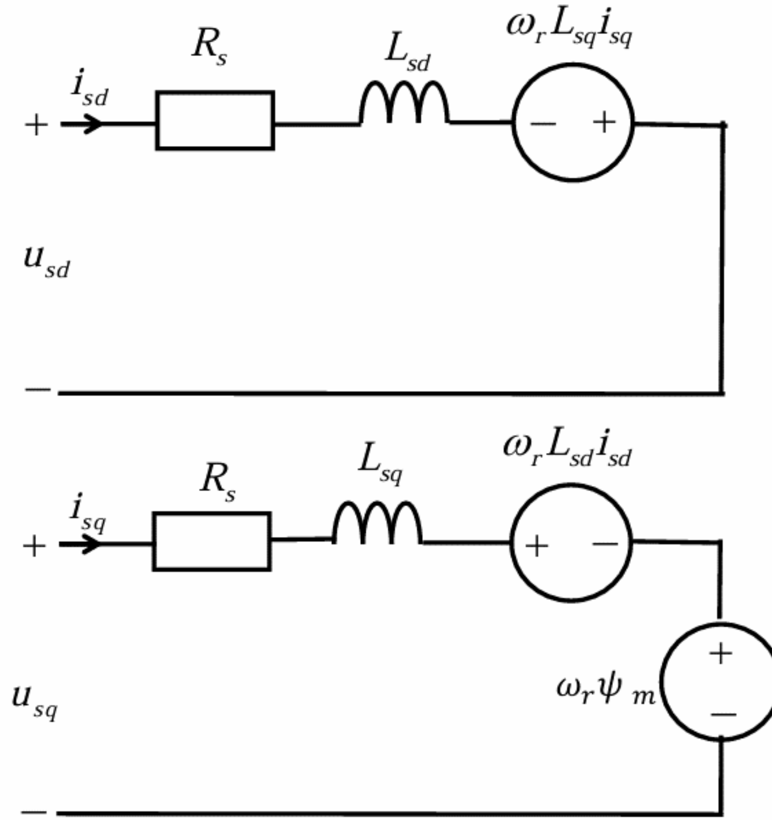

Figure 3.10: The d-q axis circuit representation of PMSM [83]

The mathematical equation of the d-q axis voltage are described below. In a Permanent Magnet Synchronous Machine (PMSM), the dq-axis model is used for analysis and control. The key variables and equations are as follows:

$$U_{sd} = R_s I_{sd} + L_d \frac{dI_{sd}}{dt} - \omega_r L_q I_{sq} \tag{3.23}$$

$$U_{sq} = R_s I_{sq} + L_q \frac{dI_{sq}}{dt} + \omega_r L_d I_{sd} + \omega_r \lambda_m \tag{3.24}$$

where: I_{sd} represents Direct axis current, I_{sq} represents Quadrature axis current U_{sd} represents Direct axis voltage, U_{sq} represents Quadrature axis voltage, R_s represents Stator resistance, $L_d$represents d-axis inductance, L_q representsq-axis inductance, ω_r represents Rotor angular velocity, λ_m represents Permanent magnet flux linkage. The flux linkage and torque equation are described as blow.

$$\lambda_{sd} = L_d I_{sd} + \lambda_m \tag{3.25}$$

$$\lambda_{sq} = L_q I_{sq} \tag{3.26}$$

$$T_e = \frac{3}{2} \cdot \frac{p}{2} \cdot (\lambda_m I_{sq} - L_d I_{sd} I_{sq}) \tag{3.27}$$

where:

- T_e: Electromagnetic torque.
- p: Number of pole pairs.

The analytic loss model parameters of peak load current, power factor, and modulation index are obtained from the machine model as follows,

$$\begin{aligned} I_{\text{peak}} &= \sqrt{I_{sd}^2 + I_{sq}^2} \\ u_{\text{peak}} &= \sqrt{u_{sd}^2 + u_{sq}^2} \\ p &= 1.5\,(I_{sd} \cdot u_{sd} + I_{sq} \cdot u_{sq}) \\ Q &= 1.5\,(u_{sq} \cdot I_{sd} - u_{sd} \cdot I_{sq}) \\ S &= \sqrt{p^2 + Q^2} \end{aligned} \tag{3.28}$$

where I_{peak} is the peak current, u_{peak} is the peak voltage, p is the active power, Q is the reactive power, S is the apparent power,I_{sd} and I_{sq} are the direct and quadrature components of the current, u_{sd} and u_{sq} are the direct and quadrature components of the voltage.From the above machine model, the following parameters for the analytic model are generated:

$$\text{Power factor} = \frac{|p|}{|S|} \tag{3.29}$$

$$m_a = \frac{u_{\text{peak}}}{u_{dc}} \cdot \frac{1}{\sqrt{3}} \tag{3.30}$$

where m_a is the modulation index,p is the active power,S is the apparent power, u_{peak} is the peak voltage,u_{dc} is the DC-link voltage.
The simulation uses two different machine types: a permanent magnet synchronous motor ,PMSM and an Electrically excited synchronous motor,EESM. For both machines, the DC-link voltage and shaft power are 360 volts with 60 kW and 800 volts with 250 kW, respectively. The inverter loss for the four different cases of machine maps is shown below.

3.8 PWM Frequancy Based Hystresis Controller

This thesis uses a hysteresis type of controller with some modifications using a reference temperature band. This controller helps to maintain constant or reduce the junction temperature cyclic stress in certain defined regions. The hysteresis controller is less complicated than others, like the PI controller, model predictive controller (MPC), and fuzzy logic. However, it provides excellent results compared to the system with no controller. The controller input and output are shown in the figure 3.11.
Therefore, its simplicity (requires only a few parameters), low cost, fast reaction (response), and good results make it optional for this work. The controller uses switching PWM frequency as controller parameters; according to the junction temperature, the switching frequency is changed to increase and decrease the switching loss since it directly impacts the switching loss, which takes the most significant proportion of the loss components. The controller compares the actual junction

temperature change, ΔT_j, with reference junction temperature change, ΔT_{j_ref}; when the difference goes up, the cyclic stress increases, and so the controller hold constant or reduce the switching frequency in order to save the lifetime, and when the difference is minimal, the controller increases the switching frequency to increase the work performance of the system.

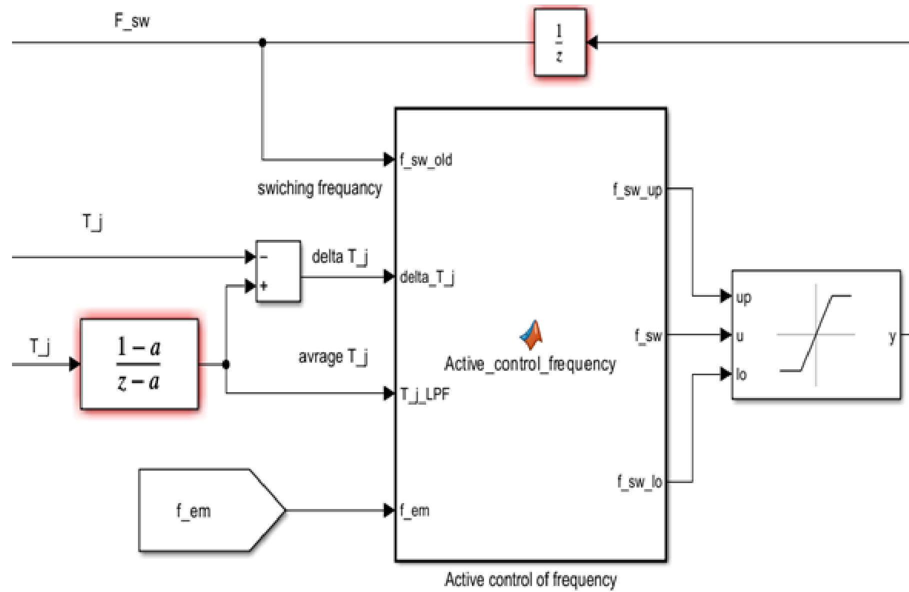

Figure 3.11: Hysteresis controller with analytic loss model integration

The actual ΔT_j is obtained by subtracting the actual T_j from the average result obtained from the low pass filter, which is connected to the actual T_j. The controller considers only switching frequency due to its fast response and easy access to the parameters instead of load current and modulation index. The controller structure is described in a block diagram, as shown in the figure 3.11.

4
Analysis of ATC via PWM frequency

This section compares results with and without the controller. The comparison is based on lifetime and efficiency considerations. Before comparison, the simulation identifies the controller's desired parameters , which gives better efficiency and life-time. The simulation uses a PMSM machine, an eight-chip hybrid pack infineon inverter module, and a truck for Si IGBT, R. Bayerer et al. (CIPS 2008) lifetime model with controller. After identifying the desired parameters, the simulation is extended to the six different lifetime models. Finally, the sensitivity analysis is done using different simulation setups such as using another hybrid pack inverter module and EESM machine model both for for Si and SiC MOSFET, R. Bayerer et al.(CIPS 2008) lifetime model and also for hybridpack SiC infineon bond wire and solder layer lifetime model.

4.1 Comparison With and Without Controller

A comparison of the with and without controllers is done using the desired controller parameters for the Si IGBT, R. Bayerer et al. (CIPS 2008) lifetime model. As the table 4.1 shows, the controller extends the lifetime by more than 500%. Table 4.1 and figure 4.1 simulation result is done by holding together the transient and cruise simulation in a cascaded way.As shown from the figure 4.1 for the first 700 second, it is transient mode and there is high-speed variation. Due to this, the power loss also varies in a wide range for the next 2000 seconds. The drive cycle source is a Cruise cycle and approximately constant speed, and the power loss shows a short range of variation.

Table 4.1: Comparison of Lifetime and Efficiency With and Without Controller Si IGBT, R. Bayerer et al. (CIPS 2008) model

Parameter	With Controller	Without Controller	Comparison
Fcuttoff	0.02 Hz	0.02 Hz	-
Delta_Tj_Ref	1°C	1°C	-
Fincrement	2 kHz	2 kHz	-
LifeTime(hours)	1.2×10^7	1.6×10^6	587.5%
Effi	0.9883	0.9853	0.3%

Again, after this time duration,it is a transient mode, and the speed and power loss

vary widely. As power and temperature are linearly related, as power varies, the junction temperature also varies, and the controller adjusts the frequency according to the power loss to maintain the junction temperature within the defined region.

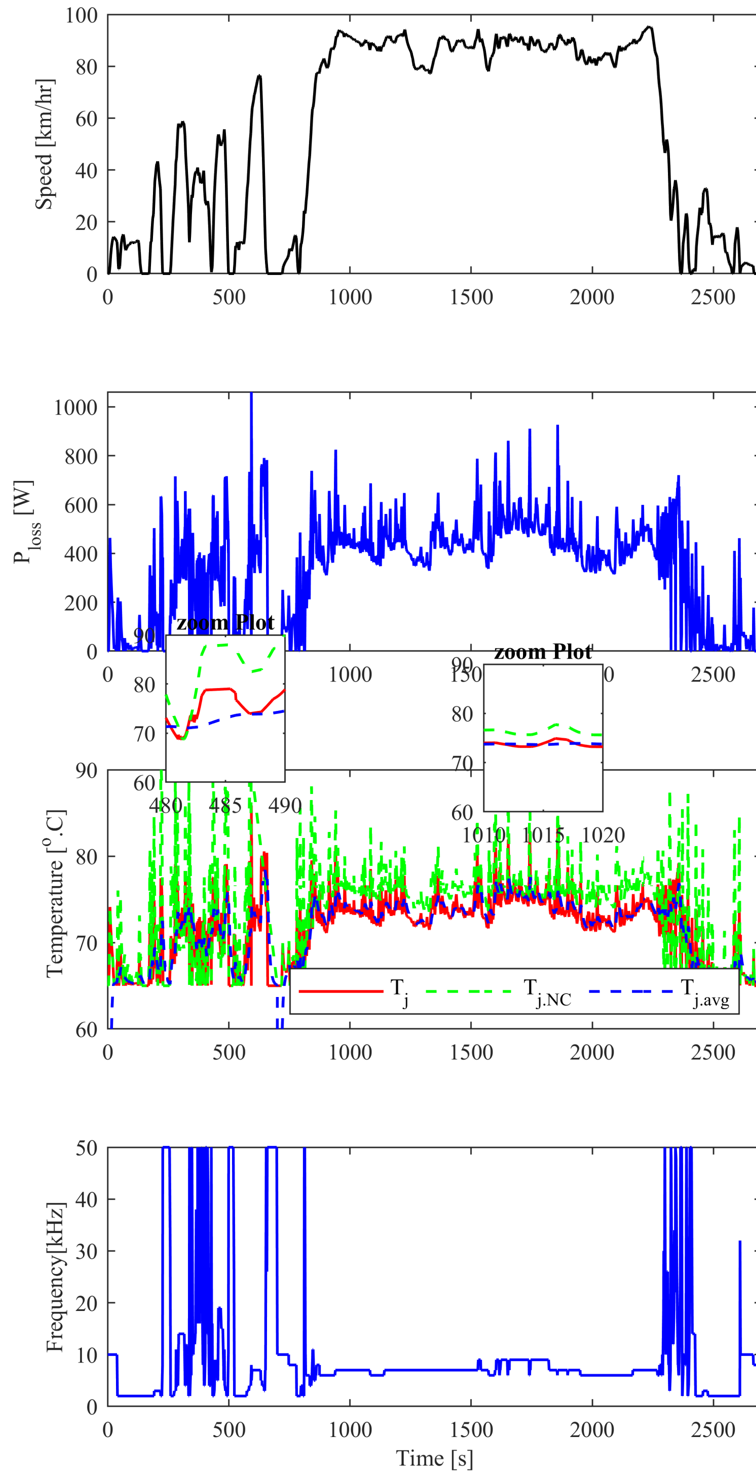

Figure 4.1: speed power, temperature and frequency

The above simulation is done by holding the transient and cruise drive cycles together. Therefore, before going to sensitivity analysis, performing the transient

mode of drive cycle results is necessary.Figure 4.2 and table 4.2 shows system result in transient mode of drive cycles.

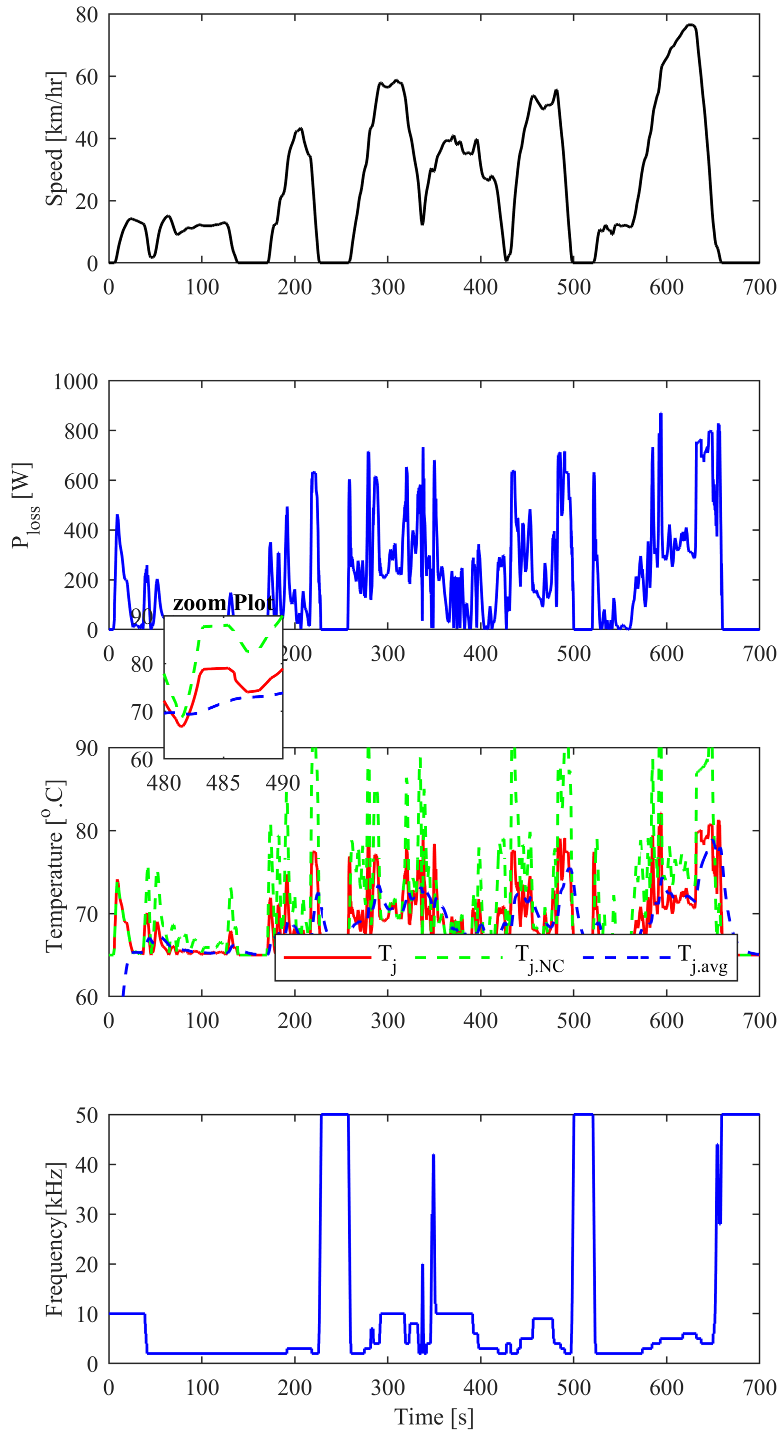

Figure 4.2: Transient mode only simulation result with controller

As shown from the figure the speed varies continuously as well the power loss. The controller adjust the switching frequency as shown in order to reduce the junction temperature.Between 200 second to 500 second the power loss swings to much up and down so the controller is busy to maintain the power loss constant.

4.2 Reference Temperature Band selection

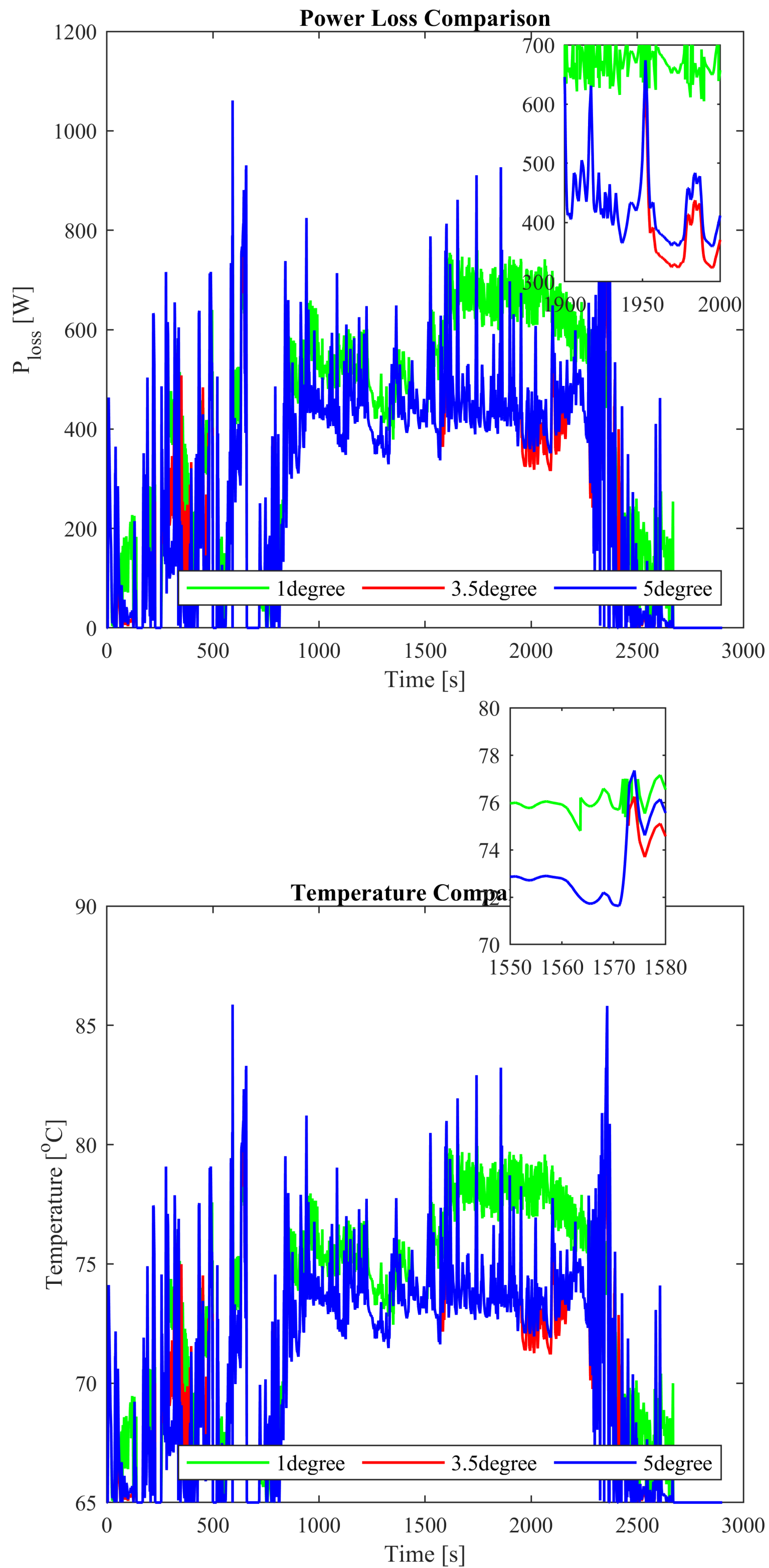

Figure 4.3: comparison of different temperature band

Table 4.2: Comparison of Lifetime and Efficiency With and Without Controller for transient model only

Parameter	With Controller	Without Controller	Comparison
Fcuttoff	0.02 Hz	0.02 Hz	-
Delta_Tj_Ref	3.5°C	3.5°C	-
Fincrement	2 kHz	2 kHz	-
LifeTime(hours)	4.9×10^6	6.19×10^5	691.5%
Effi	0.9781	0.9638	1.43%

As shown in figure 4.3 and table 4.3, the simulations use different reference temperature bands but the same low pass filter frequency and the same adjustment incremental frequency level to determine the best reference temperature band. The simulation result is shown below in the form of a table and a figure. The simulation is based on using 0.5 °C, 1 °C 2.5 °C,3.5 °C, five °C and ten °C temperatures and uses the lifetime model of Si IGBT, R. Bayerer et al. (CIPS 2008). The table 4.3 summarizes the differences. At 0.5 °C and 1.5 °C have approximately the same lifetime result but lower efficiency at one °C.

Figure 4.3 shows the power loss and junction temperature at different reference temperature bands. The figure shows that the power loss swings wildly at a five-degree temperature reference band in a wide range of gaps and the junction temperature. At 3.5 degrees, the power loss or junction temperature variation is better than the 5-degree reference but also worse than the 1-degree reference junction temperature and power loss result. A one-degree reference temperature band, resulting in power loss and junction temperature, shows the best rest as it has a smooth and short swinging range. Therefore, one °C is the desired temperature band because it provides better efficiency and longevity. Figure 4.4 shows the speed power loss, frequency, and temperature at the five °C reference temperature band.

Table 4.3: Simulation Results for Different Temperature Bands

No	Delta_Tj_Ref (°C)	Fcuttoff (Hz)	Fincrement (kHz)	Time (hours)	Efficiency
1	0.5	0.02	1	1.0696×10^7	0.9838
2	1	0.02	1	1.2000×10^7	0.9883
3	2.5	0.02	1	1.0051×10^7	0.9887
4	3.5	0.02	1	9.2058×10^6	0.9883
5	5	0.02	1	6.5485×10^6	0.9880
6	10	0.02	1	6.5485×10^7	0.9880

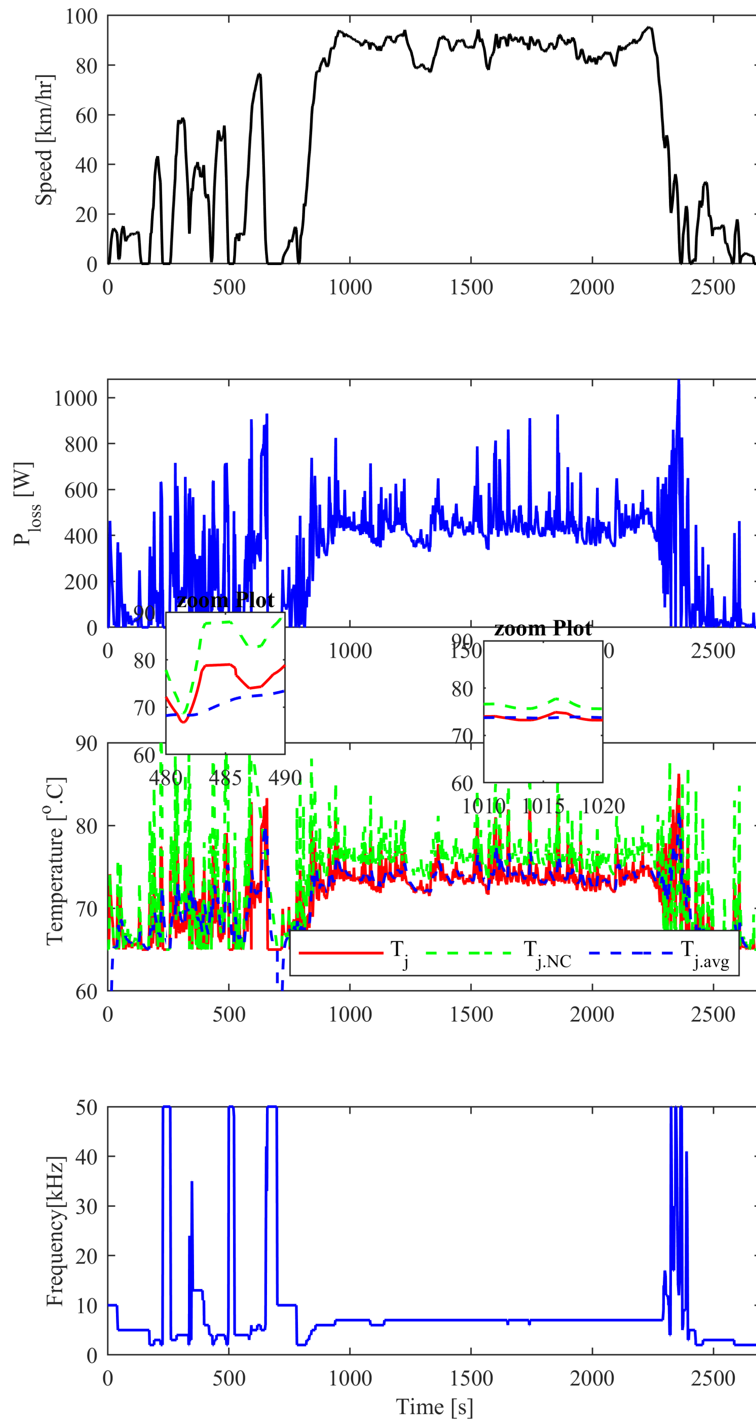

Figure 4.4: System result for 5 temperature band

4.3 Low Pass Filter Frequency selection

The previous section determines the desired reference temperature band. Now, this section analyzes the desired low pass filter cutoff frequency using this temperature band.As shown from the simulation result in table 4.5, the desired cutoff frequency is 20 mHz.

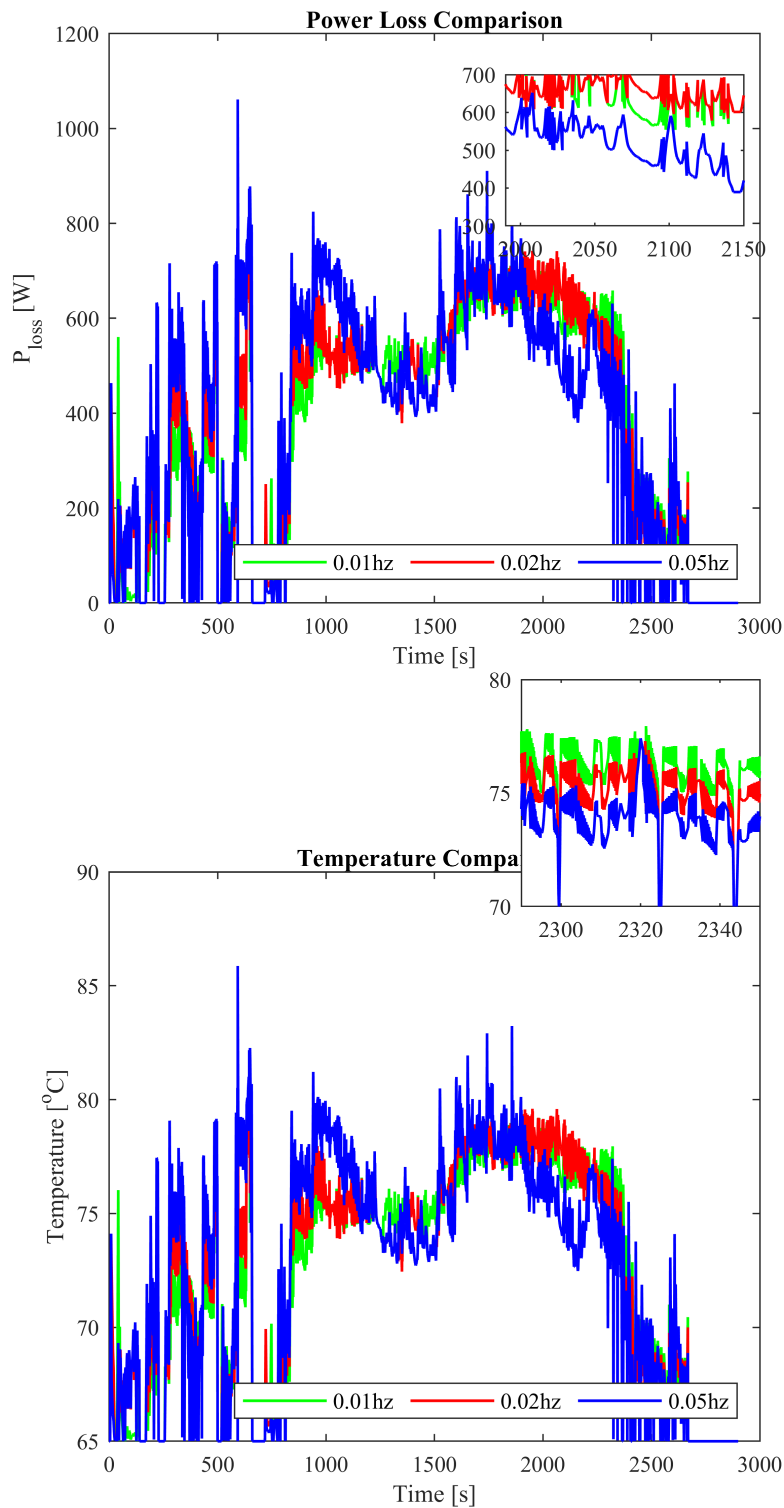

Figure 4.5: power loss and junction temperature at different cutoff frequency

Figure 4.1 shows the power loss and junction temperature result at different low pass filter cutoff frequencies. This simulation result uses a one-degree temperature reference band. Therefore, the speed fluctuation is visible in power loss and junction temperature.

Table 4.4: Simulation Result for different cutoff frequencies

No	Delta_Tj_Ref (°C)	Fcuttoff (Hz)	Fincrement (kHz)	Time (hours)	Efficiency
1	1	0.01	1	9.95×10^6	0.9886
2	1	0.02	1	1.0×10^7	0.9887
3	1	0.05	1	9.305×10^6	0.9877

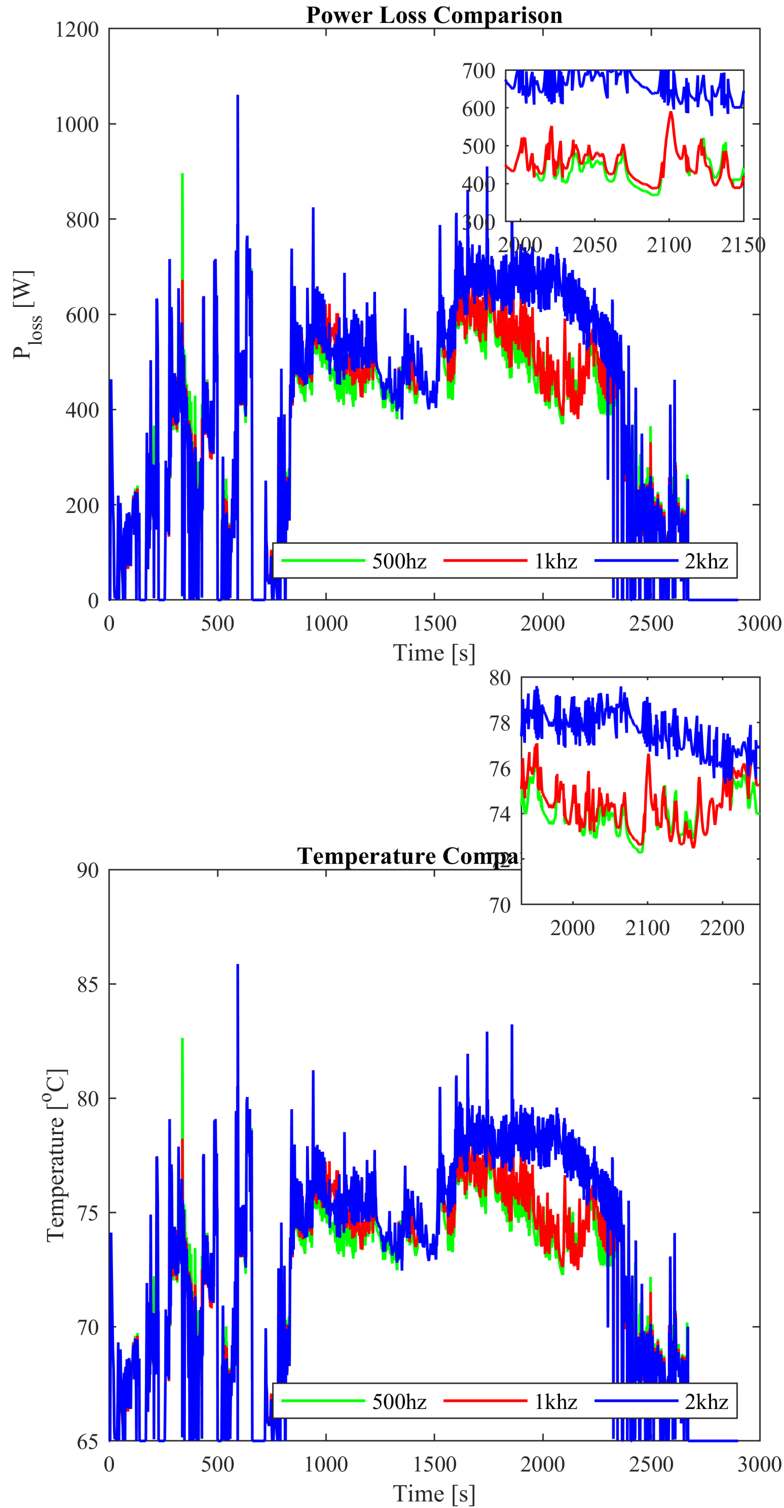

Figure 4.6: System result at different controller frequency adjustment level

This is due to the one-degree temperature reference having a lower swinging range in general for all three cases. As shown in Figure 4.1,20 mhz cutoff frequency results in a lower swinging range than the other two cases, and ten mhz shows less swinging than 50 mHz but higher cyclic stress than 20mhz. Therefore, 20 mHz is selected as the desired cutoff frequency parameter value for the following simulation tasks. Table 4.5 summarizes the three different cutoff frequency cases.

The above sections determines the reference temperature band and the low pass filter cutoff frequency.It is necessary to determine the controller frequency adjustment, increment or decrement magnitude using low pass filter frequency and temperature band.

Table 4.5: Simulation Results for different frequency increment

No	Delta_Tj_Ref (°C)	Fcuttoff (Hz)	Fincrement (kHz)	Time (hours)	Efficiency
1	1	0.02	0.5	9.86×10^6	0.9885
2	1	0.02	1	1.0×10^7	0.9887
3	1	0.02	2	1.1×10^7	0.9887

Figure 4.6 shows the power loss and junction temperature at different controller adjustment frequency increment and decrement. As in previous cases, based on the cyclic stress or swinging of the power loss and junction temperature, 500 hz and one khz provide a bit higher cyclic and stressful result than the result obtained from 2khz. From shown in the figure 4.6 and table 4.5, 2 kHz provides better result of lifetime and efficiency. Therefore, the controller desired parameters values are identified as 20 mHz, 2 kHz, and 2.5 °C, the cutoff frequency, the controller adjustment frequency increment, and ΔT_j reference , respectively.

4.4 Sensitivity Analysis

The previous section conducted all the simulations for Si IGBT, R. Bayerer et al.'s (CIPS 2008) lifetime model for PMSM machine type with an eight-chip hybrid pack Infineon power semiconductor module of the truck vehicle. In the following section, the sensitivity analysis uses a different lifetime model, another semiconductor model and a machine model.

4.4.1 Sensitivity to Different Lifetime Model

The result is generated for each of the remaining five lifetime models in terms of numbers and figures, both with and without the controller. The simulation parameters, such as cutoff frequency, the controller adjustment frequency increment, and ΔT_j reference, remain constant. Their values are 20 mHz, 2 kHz, and 2.5 °C, respectively. All lifetime models have the best efficiency and lifetime extension at those parameter values compared with other values. This shows that the lifetime of the power semiconductor depends on the controller parameters rather than the different lifetime models. This parameter test simulation result is not included here since it is similar to the steps in the previous section. The lifetime is calculated

using all the six lifetime models described in chapter three. To better understand this subsection, only the lifetime model is changed with the exact vehicle, machine, and semiconductor models used in the previous section.

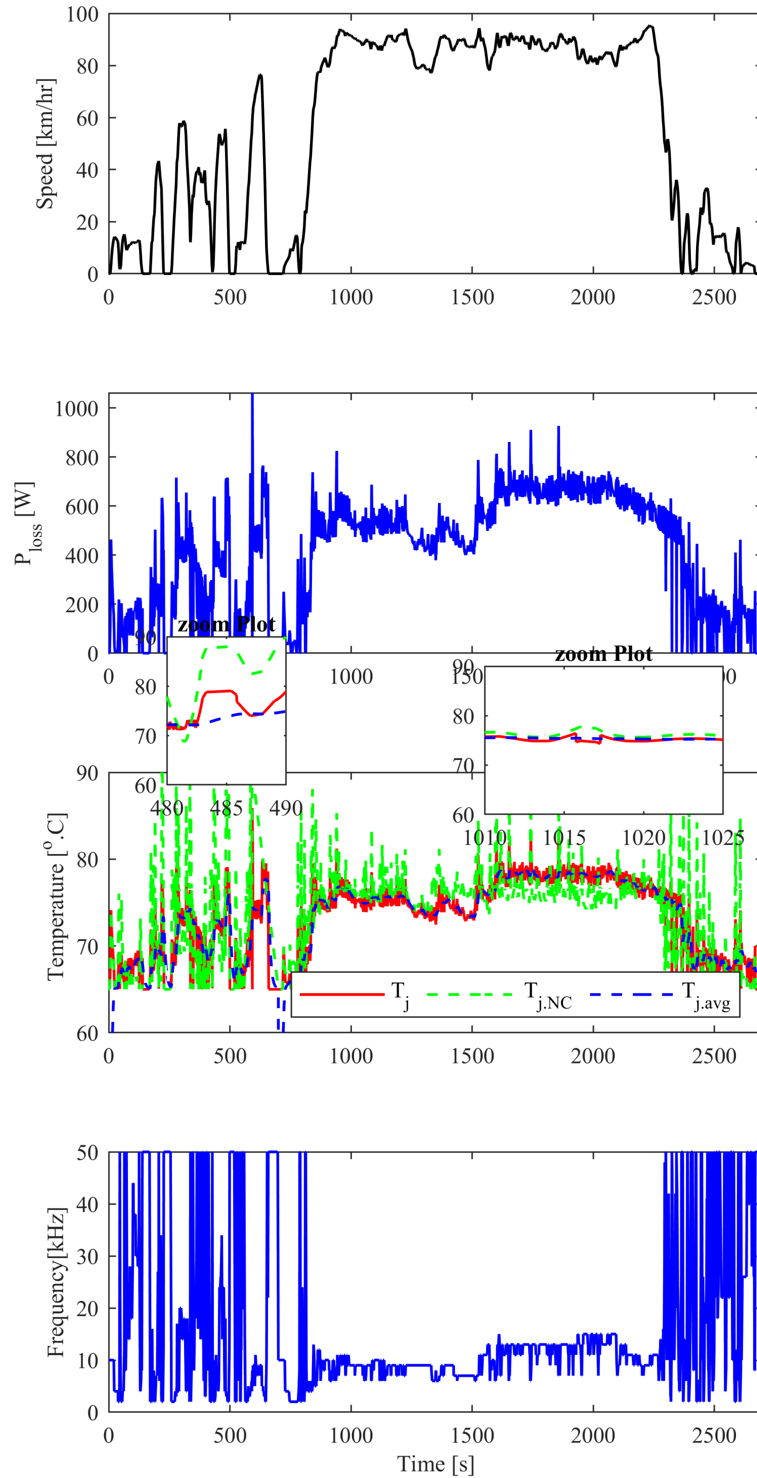

Figure 4.7: Speed, total power loss, junction and average junction temperature

Therefore, the power loss and junction temperature are the same for all lifetime

models. Due to this, the lifetime improvement result is described as a table without including the power loss and junction temperature figure for each lifetime model, and all use figure 4.7. Figure 4.7 shows speed, total power loss, junction and average junction temperature, feedback frequency used for all lifetime calculation.

Table 4.6: Comparison of Lifetime and Efficiency With and Without Controller SiC IGBT, R. Bayerer et al. (CIPS 2008) model

Parameter	With Controller	Without Controller	Comparison
Fcuttoff	0.02 Hz	0.02 Hz	-
Delta_Tj_Ref	1°C	1°C	-
Fincrement	2 kHz	2 kHz	-
Liftime (hours)	7.05×10^5	1.37×10^5	462%
Effi	0.9854	0.9853	0.01%

Table 4.7: Efficiency and lifetime comparison of IGBT with and without for Si bond wire failures Lesit Project (1997) model

Parameter	With Controller	Without Controller	Comparison
Fcuttoff	0.02 Hz	0.02 Hz	-
Delta_Tj_Ref	1°C	1°C	-
Fincrement	2 kHz	2 kHz	-
Lifetime (hours)	1.58×10^7	2.2×10^6	536.36%
Effi	0.9854	0.9853	0.01%

Table 4.8: Efficiency and lifetime comparison of IGBT with and without for Si solde layer fatigue LESIT Project (1997) model

Parameter	With Controller	Without Controller	Comparison
Fcuttoff	0.02 Hz	0.02 Hz	-
Delta_Tj_Ref	1°C	1°C	-
Fincrement	2 kHz	2 kHz	-
Lifetime (hours)	3.52×10^6	5.98×10^5	488%
Effi	0.9854	0.9853	0.01%

As shown in results from the above tables 4.6 - 4.10, the controller extended the lifetime of the power semiconductors from thousands to millions of hours, implying that the unguided or uncontrolled junction temperature variation and cyclic stress cause a significant lifetime reduction.All lifetime model shows the improvement more than 246%.

4.4.2 Sensitivity to Another Semiconductor Model

This thesis uses two different Infineon hybrid pack inverter modules to power semiconductors. Those are eight chip type (FS02MR12A8MA2B) and six chip type

Table 4.9: Efficiency and lifetime comparison of IGBT with and without controller for SiC hybridpack solder layer fatigue model

Parameter	With Controller	Without Controller	Comparison
Fcuttoff	0.02 Hz	0.02 Hz	-
Delta_Tj_Ref	1°C	1°C	-
Fincrement	2 kHz	2 kHz	-
Lifetime (hours)	4.57×10^7	2.92×10^6	246.5%
Effi	0.9854	0.9853	0.01%

Table 4.10: Efficiency and lifetime comparison of with and without controller for SiC hybridpack bond wire failure lifetime model

Parameter	With Controller	Without Controller	Comparison
Fcuttoff	0.02 Hz	0.02 Hz	-
Delta_Tj_Ref	1°C	1°C	-
Fincrement	2 kHz	2 kHz	-
Lifetime (hours)	2.63×10^8	3.98×10^7	650%
Effi	0.9854	0.9853	0.01%

modules (FS03MR12A7MA2BA) [6].In the previous section, the simulation is done using the eight-chip hybrid pack semiconductor type. Therefore, the following simulation results use the six chip semiconductors with two different lifetime models, Si and SiC MOSFET (R. Bayerer et al., CIPS 2008), for better understand the comparison of the eight chip type power semiconductor.

Table 4.11: Six chip semiconductor With and Without Controller Si IGBT, R. Bayerer et al. (CIPS 2008) model

Parameter	With Controller	Without Controller	Comparison
Fcuttoff	0.02 Hz	0.02 Hz	-
Delta_Tj_Ref	1°C	1°C	-
Fincrement	2 kHz	2 kHz	-
LifeTime(hours)	3.68×10^6	7.95×10^5	362.89%
Effi	0.9845	0.9858	0.13%

Table 4.12: Six chip semiconductor With and Without Controller SiC IGBT, R. Bayerer et al. (CIPS 2008)lifetime model

Parameter	With Controller	Without Controller	Comparison
Fcuttoff	0.02 Hz	0.02 Hz	-
Delta_Tj_Ref	1°C	1°C	-
Fincrement	2 kHz	2 kHz	-
LifeTime(hours)	2.82×10^6	7.19×10^4	382.2%
Effi	0.9845	0.9858	0.13%

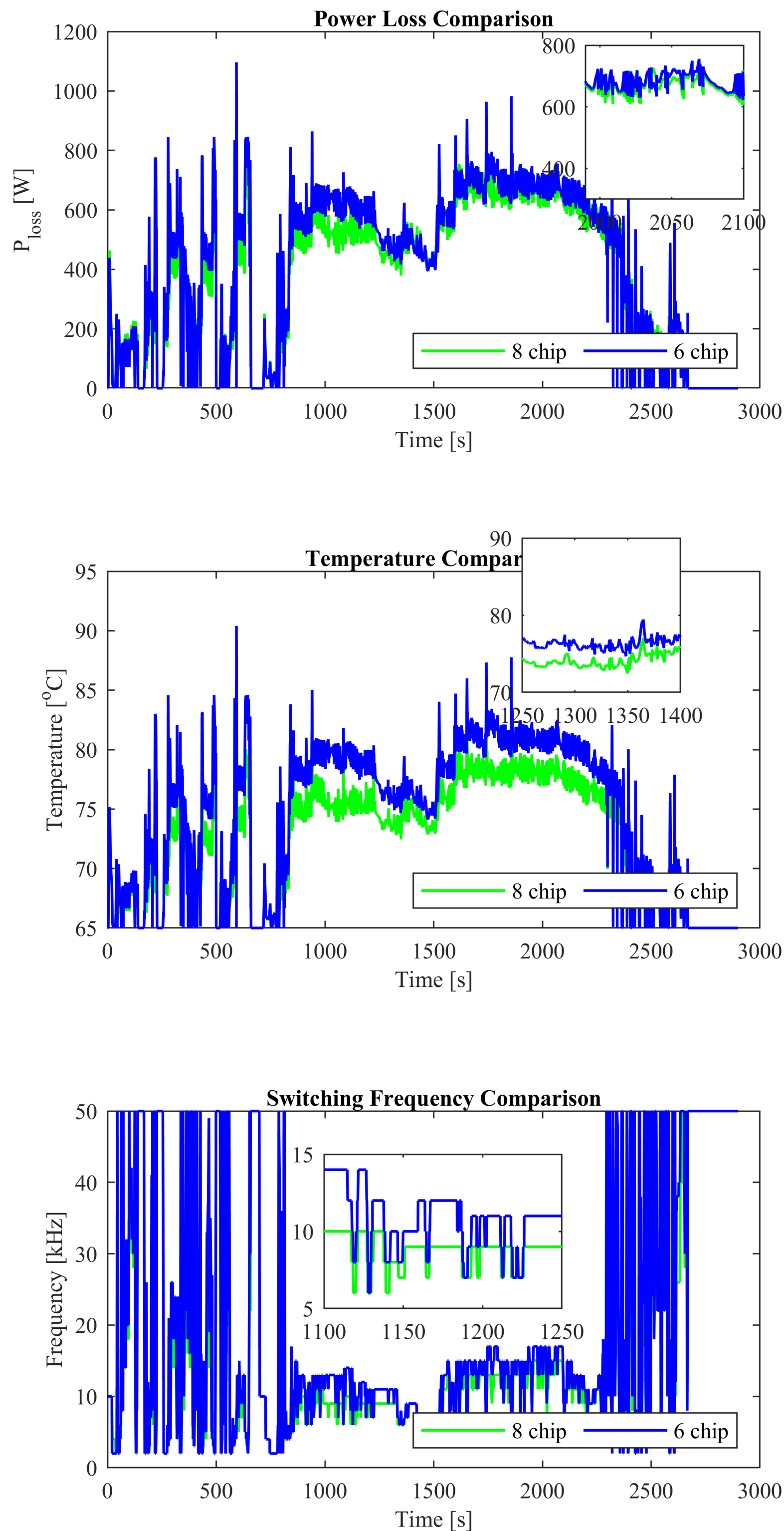

Figure 4.8: Speed, total power loss, junction for six chip semiconductor Si lifetime model

Figure 4.8 and table 4.11 show the six chip power semiconductor simulation result with and with the controller using Si IGBT, R. Bayerer et al. (CIPS 2008) lifetime model. Table 4.12 shows the six-chip power semiconductor simulation result with

and with the controller Using SiC IGBT, R. Bayerer et al. (CIPS 2008) model.As shown from the result, the extension in a lifetime and efficiency improvement is lower than the eight-chip power semiconductor, as shown in table 4.1. The power loss and junction temperature plot show that the six-chip power semiconductor has a wide range of swinging or cyclic stress as shown in figure 4.8. Therefore, the eight-chip semiconductor is less sensitive to junction temperature fluctuation.

Table 4.13: The two chips comparison using Si IGBT, R. Bayerer et al. (CIPS 2008) lifetime model

Parameter	8-Chip	6-Chip	Comparison
Fcuttoff	0.02 Hz	0.02 Hz	-
Delta_Tj_Ref	1°C	1°C	-
Fincrement	2 kHz	2 kHz	-
LifeTime(hours)	587.5%	362.89%	224.61%
Effi	0.3%	0.13%	0.17%

Table 4.14: The two chips comparison using SiC IGBT, R. Bayerer et al. (CIPS 2008) lifetime model

Parameter	8-Chip	6-Chip	difference
Fcuttoff	0.02 Hz	0.02 Hz	-
Delta_Tj_Ref	1°C	1°C	-
Fincrement	2 kHz	2 kHz	-
LifeTime(hours)	462%	382.2%	79.8%
Effi	0.3%	0.13%	0.17%

4.4.3 Sensitivity to Different Machine Model

The final case of the simulation comparison is using a different machine model. Still now, the simulation is done using a PMSM machine with 800v DC voltage and 250 watt shaft power. Another type of machine, called an electrically excited synchronized motor, EESM, is used for the following simulation with the same shaft power and DC voltage rate. The simulation uses an eight-chip semiconductor hybrid pack with the help of Si IGBT, R, Bayerer et al. (CIPS 2008) and SiC MOSFET, R. Bayerer et al., (CIPS 2008)lifetime model for easy comparison with the PMSM result in section 4.2. Again, the simulation uses the cruise and transient mode of the drive cycle and truck vehicle type.

Table 4.15: EESM With and Without Controller Si IGBT, R. Bayerer et al. (CIPS 2008)lifetime model

Parameter	With Controller	Without Controller	Comparison
Fcuttoff	0.02 Hz	0.02 Hz	-
Delta_Tj_Ref	1°C	1°C	-
Fincrement	2 kHz	2 kHz	-
LifeTime(hours)	6.57×10^6	1.872×10^6	250.96%
Effi	0.9898	0.9899	0.001%

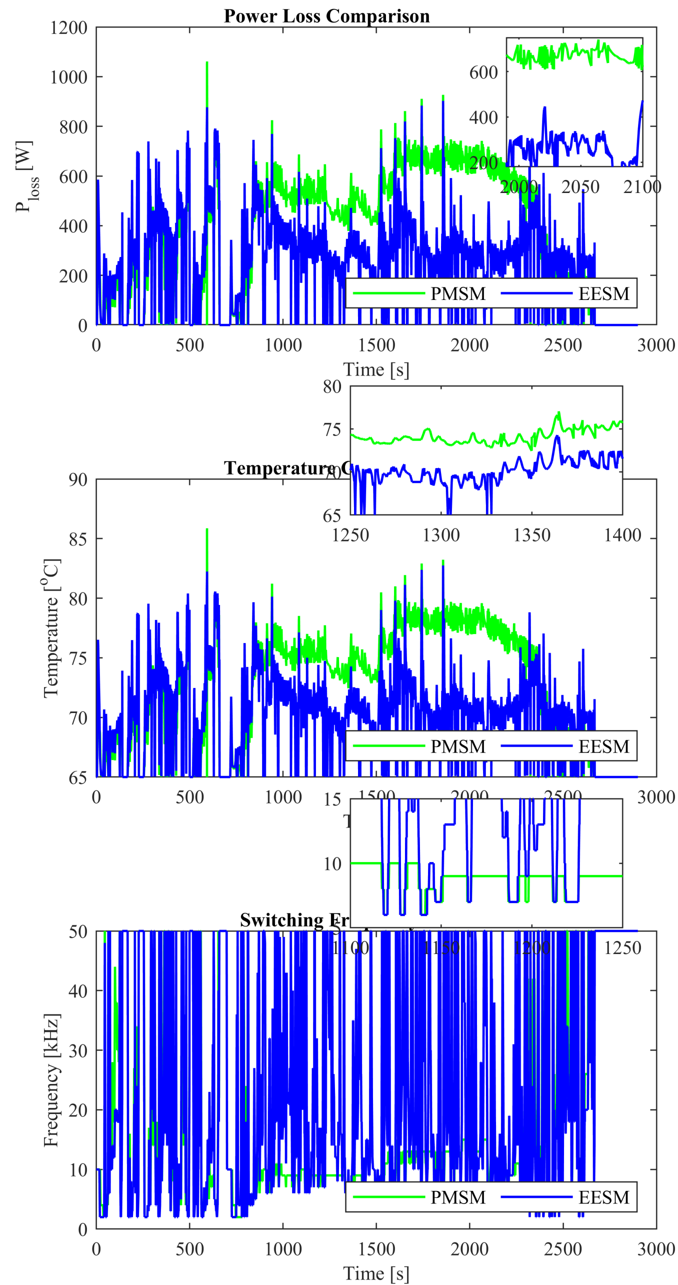

Figure 4.9: Power loss, junction temperature and frequency comparison for EESM and PMSM machine

Table 4.16 shows the EESM machine model comparison with and without the controller using SiC IGBT, R. Bayerer et al. (CIPS 2008) lifetime model. Since there is a machine model change, the power loss and junction temperature figure are different from the previous cases, as shown in Figure 4.9. As shown form the result , EESM has lower efficiency with PMSM in general and it is highly affected or sensitive than PMSM by junction temperature fluctuations seen from the figure.From zero second to end of the time range, the power loss and junction temperature varies a lot as speed varies,this creates cyclic stress and mechanical damage on the inverter.

Table 4.16: EESM With and Without Controller SiC IGBT, R. Bayerer et al. (CIPS 2008)lifetime model

Parameter	With Controller	Without Controller	Comparison
Fcuttoff	0.02 Hz	0.02 Hz	-
Delta_Tj_Ref	1°C	1°C	-
Fincrement	2 kHz	2 kHz	-
LifeTime(hours)	3.89×10^5	7.34×10^4	429.97%

Table 4.17: EESM and PMSM comparison using Si IGBT, R. Bayerer et al. (CIPS 2008)lifetime model

Parameter	PMSM	EESM	difference
Fcuttoff	0.02 Hz	0.02 Hz	-
Delta_Tj_Ref	1°C	1°C	-
Fincrement	2 kHz	2 kHz	-
LifeTime(hours)	587.5%	429.97%	157.53%
Effi	0.3%	0.001%	0.299%

Table 4.18: EESM and PMSM comparison using SiC IGBT, R. Bayerer et al. (CIPS 2008)lifetime model

Parameter	PMSM	EESM	difference
Fcuttoff	0.02 Hz	0.02 Hz	-
Delta_Tj_Ref	1°C	1°C	-
Fincrement	2 kHz	2 kHz	-
LifeTime(hours)	462%	429.97%	32.03%
Effi	0.3%	0.001%	0.299%

Table 4.17 and 4.18 compares the PMSM and EESM in terms of the improvement of each of the machines with and without the controller. As shown, EESM has lower improvement in lifetime and efficiency concerns. Therefore, it is susceptible and has a lower lifetime than PMSM.

5

Conclusion and Recommendation

5.1 Conclusion

This thesis has examined the effects of junction temperature fluctuations on power semiconductors for high-power drive applications. The study analyzes the effects of high junction temperature and wide thermal swings on device reliability, especially concerning bond wire failures and solder layer fatigue.This is done using an analytical model of power semiconductors switching and conduction losses, junction temperature thermal network model atcive thermal control stratagies and togther with various lifetime models for IGBTs and MOSFETs for comparesion.

This thesis investigated various active thermal control (ATC) strategies in the litrature section.Those are divided into software-based and hardware-based methods . This research focused on a software-based solution, particularly focusing a frequency-based hysteresis is controller. Because hardware-based ATC approaches have added space and expense constraints. Frequency-based hysteresis ATC takes advantage of the direct correlation between switching power loss and junction temperature variation. The controller is also simple to implementation and provides quick response time.

The results demonstrate that the hysteresis-based active thermal control technique effectively reduces the cyclic thermal stress on power semiconductors.The result shows significantly extending their operational lifetime. The improvement is in millions of lifetimes hours.This could lead to significant cost reduction from frequent replacements and the related expenses.

5.2 Recommendation

The lifetime improvement can be extended further by using advanced frequency modulation techniques like FT60 and incorporating future loss prediction systems, such as replacing the hysteresis control model with model predictive control techniques.

Bibliography

[1] IEA (2023), Electric car sales, 2016-2023, IEA, Paris. https://www.iea.org/data-and-statistics/charts/electric-car-sales-2016-2023, Licence: CC BY 4.0.

[2] IEA (2023), Global EV Outlook 2023, IEA, Paris. https://www.iea.org/reports/global-ev-outlook-2023, Licence: CC BY 4.0.

[3] 2024 EV forecast: the supply chain, charging network, and battery materials market.

[4] A. Acquaviva, A. Rodionov, A. Kersten, T. Thiringer, and Y. Liu, "Analytical Conduction Loss Calculation of a MOSFET Three-Phase Inverter Accounting for the Reverse Conduction and the Blanking Time," *IEEE Transactions on Industrial Electronics*, vol. 68, no. 8, pp. 6682-6691, 2021.

[5] Z. Ni, X. Lyu, O. P. Yadav, B. N. Singh, S. Zheng, and D. Cao, "Overview of Real-Time Lifetime Prediction and Extension for SiC Power Converters," *IEEE Transactions on Power Electronics*, vol. 35, pp. 7765-7794, 2020. https://api.semanticscholar.org/CorpusID:213872827

[6] Infineon Technologies, "FS02MR12A8MA2B | HybridPACK™ Drive G2 CoolSiC™ G2 module," Infineon Technologies.

[7] R. Bayerer, T. Herrmann, T. Licht, J. Lutz, and M. Feller, "Model for Power Cycling Lifetime of IGBT Modules–Various Factors Influencing Lifetime," in *2008 5th International Conference on Integrated Power Electronics Systems (CIPS)*, 2008.

[8] Z. Lu, R. Shi, Y. Li, et al., "RUL Estimation for Power Electronic Devices Based on LESIT Equation," in *2023 Prognostics and Health Management Conference (PHM)*, 2023.

[9] M. Thoben, "Reliability and Lifetime of Power Modules," Infineon Technologies, Max Planck Str. 1, D-59581 Warstein.

[10] J. Kuprat, C. H. van der Broeck, M. Andresen, S. Kalker, M. Liserre, and R. W. De Doncker, "Research on Active Thermal Control: Actual Status and Future Trends," *IEEE Journal of Emerging and Selected Topics in Power Electronics*, vol. 9, no. 6, pp. 6494-6506, 2021. doi: 10.1109/JESTPE.2021.3067782.

[11] Z. Ni, X. Lyu, O. P. Yadav, B. N. Singh, S. Zheng, and D. Cao, "Overview of Real-Time Lifetime Prediction and Extension for SiC Power Converters," *IEEE Transactions on Power Electronics*, vol. 35, no. 8, pp. 7765-7794, 2020. doi: 10.1109/TPEL.2019.2962503.

[12] B. J. Baliga, "Planar Power MOSFETs," in *Silicon Carbide Power Devices*, Singapore: World Scientific, 2005, ch. 9, p. 242.

[13] R. Singh, “Reliability and Performance Limitations in SiC Power Devices,” *Microelectronics Reliability*, vol. 46, no. 5/6, pp. 713–730, 2006.

[14] L. Yu, K. P. Cheung, J. Campbell, J. S. Suehle, and K. Sheng, "Oxide Reliability of SiC MOS Devices," in *2008 IEEE International Integrated Reliability Workshop Final Report*, pp. 141-144, 2008. doi: 10.1109/IRWS.2008.4796106.

[15] S. K. Gupta, J. Singh, and J. Akhtar, “Materials and Processing for Gate Dielectrics on Silicon Carbide (SiC) Surface,” in *Physics and Technology of Silicon Carbide Devices*, Rijeka, Croatia: IntechOpen, 2012, ch. 8, pp. 207–234.

[16] I. Yonenaga, "Hardness of Bulk Single-Crystal GaN and AlN," *MRS Internet Journal of Nitride Semiconductor Research*, vol. 7, no. 6, 2002.

[17] I. Kovacevic-Badstuebner, J. W. Kolar, and U. Schilling, "Modelling for the Lifetime Prediction of Power Semiconductor Modules," in *Proceedings of the 2015 International Conference on Power Electronics and Applications*, 2015. Available: `https://api.semanticscholar.org/CorpusID:113669484`.

[18] R. Singh and A. R. Hefner, "Reliability of SiC MOSFET Devices," *Solid-State Electronics*, vol. 48, no. 10-11, pp. 1717-1720, 2004.`https://www.sciencedirect.com/science/article/pii/S0038110104001406`.

[19] X. Jiang, J. Wang, J. Lu, J. Chen, X. Yang, Z. Li, C. Tu, and Z. J. Shen, "Failure Modes and Mechanism Analysis of SiC MOSFET Under Short-Circuit Conditions," *Microelectronics Reliability*, vol. 88-90, pp. 593-597, 2018.`https://www.sciencedirect.com/science/article/pii/S002627141830667X`.

[20] X. Ye, C. Chen, Y. Wang, G. Zhai, and G. J. Vachtsevanos, "Online Condition Monitoring of Power MOSFET Gate Oxide Degradation Based on Miller Platform Voltage," *IEEE Transactions on Power Electronics*, vol. 32, no. 6, pp. 4776–4784, Jun. 2017.

[21] U. Karki and F. Z. Peng, "Effect of Gate Oxide Degradation on Electrical Parameters of Power MOSFETs," *IEEE Transactions on Power Electronics*, vol. 33, no. 12, pp. 10764–10773, Dec. 2018.

[22] A. J. Lelis, R. Green, D. B. Habersat, and M. El, "Basic Mechanisms of Threshold-Voltage Instability and Implications for Reliability Testing of SiC MOSFETs," *IEEE Transactions on Electron Devices*, vol. 62, no. 2, pp. 316–323, Feb. 2015.

[23] R. Ouaida, B. Rougier, E. N. D. Tognini, P. W. S. Soares, and E. K. M. F. Schmitz, "Gate Oxide Degradation of SiC MOSFET in Switching Conditions," *IEEE Electron Device Letters*, vol. 35, no. 12, pp. 1284–1286, Dec. 2014.

[24] E. Ugur, F. Yang, S. Pu, S. Zhao, and B. Akin, "Degradation Assessment and Precursor Identification for SiC MOSFETs Under High Temp Cycling," *IEEE Transactions on Industrial Applications*, vol. 55, no. 3, pp. 2858–2867, May/Jun. 2019.

[25] Z. Pavlovic et al., "Influence of Gate Oxide Charge Density on VDMOS Transistor ON-Resistance," in *Proceedings of the International Conference on Microelectronics*, vol. 2, pp. 663–666, 1999.

[26] C. Chen, X. Ye, Y. Wang, J. Xu, and G. Zhai, "PHM Application of Power Converters Using Health Precursor of Power MOSFETs," in *Proceedings of the Prognostics and Health Management Conference*, pp. 1–5, 2015.

[27] G. Liu, B. R. Tuttle, and S. Dhar, "Silicon Carbide: A Unique Platform for Metal-Oxide-Semiconductor Physics," *Applied Physics Reviews*, vol. 2, no. 2, Art. no. 021307, 2015.

[28] A. Agarwal, H. Fatima, S. Haney, and S. H. Ryu, "A New Degradation Mechanism in High-Voltage SiC Power MOSFETs," *IEEE Electron Device Letters*, vol. 28, no. 7, pp. 587–589, Jul. 2007

[29] "SiC Power Devices and Modules," ROHM Semiconductor, Kyoto, Japan, Application Note, 2013.

[30] R. Bonyadi, O. Alatise, S. Jahdi, J. Hu, L. Evans, and P. A. Mawby, "Investigating the Reliability of SiC MOSFET Body Diodes Using Fourier Series Modelling," in *Proceedings of the IEEE Energy Conversion Congress and Expo*, pp. 443–448, 2014.

[31] T. Kimoto and J. A. Cooper, "Device Processing of Silicon Carbide," in *Fundamentals of Silicon Carbide Technology—Growth, Characterization, Devices, and Applications*, 1st ed. Hoboken, NJ, USA: Wiley, 2014, p. 241.

[32] Y. Wang, X. Dai, G. Liu, Y. Wu, D. Li, and S. Jones, "Status and trend of SiC power semiconductor packaging," in *Proceedings of the 16th International Conference on Electronic Packaging Technology*, 2015, pp. 396–402.

[33] V. Mulpuri, "Failure analysis and high temperature characterization of silicon carbide power MOSFETs," M.S. thesis, Dept. Elect. Comput. Eng., Univ. Akron, Akron, OH, USA, 2017.

[34] M. Held, P. Jacob, G. Nicoletti, P. Scacco, and M. Poech, "Fast power cycling test of IGBT modules in traction application," in *Proceedings of the 2nd International Conference on Power Electronics and Drive Systems*, 1997, vol. 1, pp. 425–430.

[35] J. McPherson, "Time-to-failure models for selected failure mechanisms," in *Reliable Physics and Engineering: Time-to-Failure Modeling*, 2nd ed., Basel, Switzerland: Springer, 2013, p. 159.

[36] H. Luo, F. Iannuzzo, N. Baker, F. Blaabjerg, W. Li, and X. He, "Study of current density influence on bond wire degradation rate in SiC MOSFET modules," *IEEE Journal of Emerging and Selected Topics in Power Electronics*, to be published.

[37] W. Chen, L. Zhang, P. Krishna, A. M. Bazzi, S. Joshi, and E. M. Dede, "Data-driven approach for fault prognosis of SiC MOSFETs," *IEEE Transactions on Power Electronics*, to be published.

[38] A. Volke and M. Hornkamp, "Type tests and routine tests," in *IGBT Modules—Technologies, Driver, and Application*, Neubiberg, Germany: Infineon Technologies, 2012, p. 509.

[39] M. Ciappa, "Selected failure mechanisms of modern power modules," *Microelectronics Reliability*, vol. 42, no. 4/5, pp. 653–667, 2002.

[40] A. Hamidi, N. Beck, K. Thomas, and E. Herr, "Reliability and lifetime evaluation of different wire bonding technologies for high power IGBT modules," *Microelectronics Reliability*, vol. 39, no. 6/7, pp. 1153–1158, 1999.

[41] P. Nayak, S. K. Pramanick, and K. Rajashekara, "A high-temperature gate driver for silicon carbide MOSFET," *IEEE Transactions on Industrial Electronics*, vol. 65, no. 3, pp. 1955–1964, Mar. 2018.

[42] N. Baker, T. Benick, and F. Blaabjerg, "Test setup for long-term reliability investigation of silicon carbide MOSFETs," in *Proceedings of the 15th European Conference on Power Electronics and Applications*, 2013, pp. 1–9.

[43] K. Li, G. Y. Tian, L. Cheng, A. Yin, W. Cao, and S. Crichton, "State detection of bond wires in IGBT modules using eddy current pulsed thermography," *IEEE Transactions on Power Electronics*, vol. 29, no. 9, pp. 5000–5009, Sep. 2014.

[44] W. Lai, H. Luo, F. Iannuzzo, N. Baker, and F. Blaabjerg, "Experimental investigation on the effects of narrow junction temperature cycles on die-attach solder layer in an IGBT module," *IEEE Transactions on Power Electronics*, vol. 32, no. 2, pp. 1431–1441, Feb. 2017.

[45] H. Luo, F. Iannuzzo, and F. Blaabjerg, "Solder layer degradation measurement for SiC-MOSFET modules under accelerated power cycling conditions," in *Proceedings of the 10th International Conference on Integrated Power Electronics Systems (CIPS)*, 2018.

[46] J. Lemmens, P. Vanassche, and J. Driesen, "Optimal control of traction motor drives under electrothermal constraints," *IEEE Journal of Emerging and Selected Topics in Power Electronics*, vol. 2, no. 2, pp. 249–263, Jun. 2014.

[47] V. Blasko, R. Lukaszewski, and R. Sladky, "On-line thermal model and thermal management strategy of a three-phase voltage source inverter," in *Proceedings of the 34th IAS Annual Meeting Conference Record of the Industry Applications Conference*, 1999, vol. 2, pp. 1423–1431.

[48] M. Andresen et al., "Junction Temperature Control for More Reliable Power Electronics," *IEEE Transactions on Power Electronics*, vol. 33, no. 1, pp. 80–90, Jan. 2018.

[49] T. Weckert and J. Roth-Stielow, "Lifetime as a control variable in power electronic systems," in *Proceedings of the Emobility Electr. Power Train*, Nov. 2010, pp. 1–6.

[50] C. H. van der Broeck, L. A. Ruppert, R. D. Lorenz, and R. W. De Doncker, "Methodology for active thermal cycle reduction of power electronic modules," *IEEE Transactions on Power Electronics*, vol. 34, no. 8, pp. 8213–8229, Aug. 2019.

[51] V. Blasko, "On Line Thermal Model and Thermal Management Strategy of a Three Phase Voltage Source Inverter," in *Proceedings of the IEEE Industry Applications Conference*, 1999, vol. 2, pp. 1423–1431.

[52] D. Murdock, J. Torres, J. Connors, and R. Lorenz, "Active thermal control of power electronic modules," *IEEE Transactions on Industry Applications*, vol. 42, no. 2, pp. 552–558, Mar. 2006.

[53] D. A. Murdock, "Active Thermal Control of Power Electronic Modules," *IEEE Transactions on Industry Applications*, vol. 42, no. 2, Mar./Apr. 2006.

[54] I. Vernica et al., "Modelling and Design of Active Thermal Controls for Power Electronics of Motor Drive Applications," in *Proceedings of the IEEE International Electric Machines Drives Conference (IEMDC)*, 2017, pp. 1–6.

[55] T. Bruckner and D. G. Holmes, "Optimal pulse width modulation for three-level inverters," in *Proceedings of the IEEE 34th Annual Power Electronics Specialist Conference (PESC '03)*, vol. 1, Jun. 2003, pp. 165–170.

[56] K. S. Gowri et al., “Direct torque control of induction motor based on advanced discontinuous PWM algorithm for reduced current ripple,” *Springer-Verlag*, Oct. 2010.

[57] L. Wei et al., “Analysis of PWM Frequency Control to Improve the Lifetime of PWM Inverter,” *IEEE Transactions on Industry Applications*, vol. 47, no. 2, pp. 922–930, Mar./Apr. 2011.

[58] J. Falck, “Active Thermal Control of IGBT Power Electronic Converters,” in *Proceedings of the IECON 2015 - Yokohama*, Nov. 2015, pp. 1–6.

[59] T. A. Polom, B. Wang, and R. D. Lorenz, “Control of junction temperature and its rate of change at thermal boundaries via precise loss manipulation,” *IEEE Transactions on Industry Applications*, vol. 53, no. 5, pp. 4796–4806, Sep. 2017.

[60] M. Andresen et al., “Active Thermal Control of Isolated Soft Switching DC/DC Converters,” in *Proc. IEEE*, 2016, pp. 1-7.

[61] C. H. et al., “Methodology for Active Thermal Cycle Reduction of Power Electronic Modules,” *IEEE Trans. Power Electron.*, 2018.

[62] A. Soldati, F. Dossena, G. Pietrini, D. Barater, C. Concari, and F. Iannuzzo, “Thermal stress mitigation by active thermal control: Architectures, models and specific hardware,” in *Proc. IEEE Energy Convers.*, 2017, pp. 1-5.

[63] C. Ludecke, “Balancing the Switching Losses of Paralleled SiC MOSFETs Using a Stepwise Gate Driver,” in *Proc. IEEE Energy Conversion Congress and Exposition*, 2021, pp. 1-8.

[64] B. Wang, L. Zhou, Y. Zhang, K. Wang, X. Du, and P. Sun, “Active junction temperature control of IGBT based on adjusting the turn-off trajectory,” *IEEE Trans. Power Electron.*, vol. 33, no. 7, pp. 5811–5823, Jul. 2018.

[65] A. Soldati, F. Iannuzzo, C. Concari, D. Barater, and F. Blaabjerg, “Active thermal control by controlled shoot-through of power devices,” in *Proc. 43rd Annu. Conf. IEEE*, Oct. 2017, pp. 4363–4368.

[66] J. Brandelero, J. Ewanchuk, N. Degrenne, and S. Mollov, "Lifetime extension through Tj equalisation by use of intelligent gate driver with multi-chip power module," *Microelectronics Reliability*, vols. 88–90, pp. 428–432, Sep. 2018.

[67] X. Wang, “Observer based temperature control for reduced thermal cycling in power electronic cooling,” *Elsevier*, 2013.

[68] M. Novak, V. N. Ferreira, M. Andresen, T. Dragicevic, F. Blaabjerg, and M. Liserre, "FS-MPC algorithm for optimized operation of a hybrid active neutral point clamped converter," in *Proc. IEEE Energy Convers. Congr. Expo. (ECCE)*, Sep. 2019, pp. 1447–1453.

[69] Y. Yerasimou, “Liquid Metal Magnetohydrodynamic Pump for Junction Temperature Control of Power Modules,” *IEEE Trans. Power Electron.*, vol. 33, no. 12, Dec. 2018.

[70] D. A. Murdock, J. E. Ramos, J. J. Connors, and R. D. Lorenz, “Active thermal control of power electronics modules,” in *Proc. 38th IAS Annu. Meeting Conf. Rec. Ind. Appl. Conf.*, vol. 3, Oct. 2003, pp. 1511–1515.

[71] D. Kaczorowski and A. Mertens, “Reduction of the EV inverter chip size at constant reliability by active thermal control,” in *Proc. IEEE Vehicle Power Propuls. Conf. (VPPC)*, Oct. 2016, p. 1.

[72] M. Andresen, G. Buticchi, J. Falck, M. Liserre, and O. Muehlfeld, "Active thermal management for a single-phase h-Bridge inverter employing switching frequency control," in *Proc. PCIM Eur.*, May 2015, pp. 1–8.

[73] M. Andresen, G. Buticchi, and M. Liserre, "Thermal stress analysis and MPPT optimization of photovoltaic systems," *IEEE Trans. Ind. Electron.*, vol. 63, no. 8, pp. 4889–4898, Aug. 2016.

[74] J. Wolfle, O. Lehmann, and J. Roth-Stielow, "A novel control method to improve the reliability of traction inverters for permanent magnet synchronous machines," in *Proc. IEEE 11th Int. Conf. Power Electron. Drive Syst.*, Jun. 2015, pp. 379–384.

[75] Y. Ko, M. Andresen, G. Buticchi, and M. Liserre, "Discontinuous modulation-based active thermal control of power electronic modules in wind farms," *IEEE Trans. Power Electron.*, vol. 34, no. 1, pp. 301–310, Jan. 2019.

[76] J. Wolfle, M. Nitzsche, J. Weimer, M. Stempfle, and J. Roth-Stielow, "Temperature control system using a hybrid discontinuous modulation technique to improve the lifetime of IGBT power modules," in *Proc. 18th Eur. Conf. Power Electron. Appl. (EPE ECCE Eur.)*, Sep. 2016, pp. 1–10.

[77] M. Weckert and J. Roth-Stielow, "Chances and limits of a thermal control for a three-phase voltage source inverter in traction applications using permanent magnet synchronous or induction machines," in *Proc. 14th Eur. Conf. Power Electron. Appl. (EPE)*, Aug. 2011, pp. 1–10.

[78] J. Falck, M. Andresen, and M. Liserre, "Thermal-based finite control set model predictive control for IGBT power electronic converters," in *Proc. IEEE Energy Convers. Congr. Expo. (ECCE)*, Sep. 2016, pp. 1–7.

[79] J. Falck, G. Buticchi, and M. Liserre, "Thermal stress based model predictive control of electric drives," *IEEE Trans. Ind. Appl.*, vol. 54, no. 2, pp. 1513–1522, Mar. 2018.

[80] A. Khoshkbar, et al., "Analytical Determination of Conduction and Switching Power Losses in Flying-Capacitor-Based Active Neutral-Point-Clamped Multilevel Converter," *IEEE Trans. Power Electron.*, vol. 31, no. 8, pp. xxxx-xxxx, Aug. 2016.

[81] N. Sharma, "Design, Modeling, and Verification of Distributed Electric Drivetrains," *PhD Thesis, Chalmers University of Technology*, Gothenburg, Sweden, 2022.

[82] MathWorks, "Rainflow Cycle Counting," *MathWorks Documentation*, [Online]. Available: https://se.mathworks.com/help/signal/ref/rainflow.html. [Accessed: Aug. 21, 2024].

[83] S. Lundberg, "Electric Drive Systems, Lecture 7 and 8," *Course ENM076, Chalmers University of Technology*, Gothenburg, Sweden, 2022/2023.

A
Appendix 1

This appendix contains equation used for lifetime analysis.

Si IGBT, R. Bayerer et al. (CIPS 2008) model

$$N_f = K'_{\mathrm{Si}} \cdot (\Delta T_j)^{\beta_{1,\mathrm{Si}}} \cdot \exp\left(\frac{\beta_{2,\mathrm{Si}}}{T_{vj_min,\mathrm{Si}}}\right) \cdot (I_{bw,\mathrm{Si}})^{\beta_{4,\mathrm{Si}}}$$

Si IGBT bond wire failures Lesit Project (1997) MODEL

$$N_f = A_{BW} \cdot (\Delta T_j)^{\alpha_{BW}} \cdot \exp\left(\frac{E_{a,BW}}{k \cdot T_{j_mean_K}}\right)$$

Si solder layer fatigue Si IGBT Lesit Project (1997) MODEL

$$N_f = A_{SL} \cdot (\Delta T_j)^{\alpha_{SL}} \cdot \exp\left(\frac{E_{a,SL}}{k \cdot T_{j_mean_K}}\right)$$

SiC Bond wire failures and SiC solder layer failures hybridpack MOSFET

$$N_f = A_{BW} \cdot (\Delta T_j)^{\alpha_{BW}} \cdot \exp\left(\frac{E_{a,BW}}{k \cdot T_{j_mean_K}}\right)$$

SiC MOSFET, R. Bayerer et al. (CIPS 2008) model

$$N_f = K'_{\mathrm{SiC}} \cdot (\Delta T_j)^{\beta_{1,\mathrm{SiC}}} \cdot \exp\left(\frac{\beta_{2,\mathrm{SiC}}}{T_{vj_min,\mathrm{SiC}}}\right) \cdot (I_{bw,\mathrm{SiC}})^{\beta_{4,\mathrm{SiC}}}$$

DEPARTMENT OF ELECTRICAL POWER ENGINEERING
CHALMERS UNIVERSITY OF TECHNOLOGY
Gothenburg, Sweden
www.chalmers.se

CHALMERS
UNIVERSITY OF TECHNOLOGY